Journal of Medicinal Chemistry

Article

pubs.acs.org/jmc

Structure Guided Lead Generation for *M. tuberculosis* Thymidylate Kinase (Mtb TMK): Discovery of 3-Cyanopyridone and 1,6-Naphthyridin-2-one as Potent Inhibitors

Maruti Naik,[†] Anandkumar Raichurkar,[†] Balachandra S. Bandodkar,[†] Begur V. Varun,[†] Shantika Bhat,[†] Rajesh Kalkhambkar,[†] Kannan Murugan,[†] Rani Menon,[†] Jyothi Bhat,[‡] Beena Paul,[‡] Harini Iyer,[‡] Syeed Hussein,[§] Julie A. Tucker,[§,⊥] Martin Vogtherr,[§] Kevin J. Embrey,[§] Helen McMiken,[§] Swati Prasad,[∥] Adrian Gill,[§] Bheemarao G. Ugarkar,[†] Janani Venkatraman,[‡] Jon Read,*[,§] and Manoranjan Panda*[,†]

[†]Department of Chemistry, and [‡]Department of Bioscience, Innovative Medicines Infection, AstraZeneca India Pvt. Ltd., Bellary Road, Hebbal, Bangalore, Karnataka 560024, India

[§]Discovery Sciences, Innovative Medicines, AstraZeneca, Alderley Park, Mereside, Cheshire, SK10 4TG, United Kingdom

[∥]Department of Bioscience, Innovative Medicines Infection, AstraZeneca, 35 Gatehouse Drive, Waltham, Massachusetts 02451, United States

Supporting Information

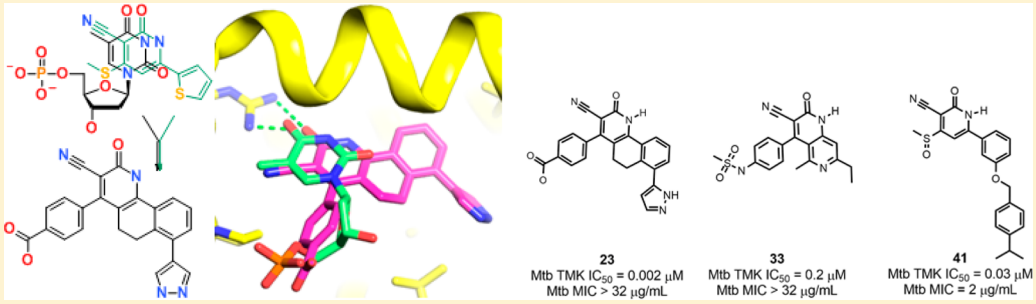

ABSTRACT: *M. tuberculosis* thymidylate kinase (Mtb TMK) has been shown in vitro to be an essential enzyme in DNA synthesis. In order to identify novel leads for Mtb TMK, we performed a high throughput biochemical screen and an NMR based fragment screen through which we discovered two novel classes of inhibitors, 3-cyanopyridones and 1,6-naphthyridin-2-ones, respectively. We describe three cyanopyridone subseries that arose during our hit to lead campaign, along with cocrystal structures of representatives with Mtb TMK. Structure aided optimization of the cyanopyridones led to single digit nanomolar inhibitors of Mtb TMK. Fragment based lead generation, augmented by crystal structures and the SAR from the cyanopyridones, enabled us to drive the potency of our 1,6-naphthyridin-2-one fragment hit from 500 μM to 200 nM while simultaneously improving the ligand efficiency. Cyanopyridone derivatives containing sulfoxides and sulfones showed cellular activity against *M. tuberculosis*. To the best of our knowledge, these compounds are the first reports of non-thymidine-like inhibitors of Mtb TMK.

INTRODUCTION

There is an urgent need for new drugs for tuberculosis (TB) with novel modes of action to combat the life-threatening multidrug resistant TB.[1] The complete genome sequencing of *Mycobacterium tuberculosis* (Mtb) followed by a series of seminal works to determine gene essentiality has opened up new targets for lead generation.[2] Additionally, the mode of action studies for the novel hits and leads emerged from phenotypic screenings utilizing methods such as resistant mutant mapping, proteomics followed by biochemical studies have played equally important role in delivering novel targets for TB drug discovery.[3] Mtb thymidylate kinase (Mtb TMK) is one of the essential targets that came from the first approach. Mtb TMK is involved in DNA synthesis and is reported to be an essential target for the survival of the mycobacterium.[4] Furthermore, Mtb TMK is amenable to biochemical and biophysical studies, and several crystal structures of complexes with TMP and other close analogs have been reported.[5] This makes it an attractive target for structure based drug design. In Gram positive pathogens such as *Streptococcus pneumoniae* and *Staphylococcus aureus*, inhibition of TMK has resulted in in vivo efficacy in mouse as demonstrated in a lead optimization program.[6] Lead generation efforts against TMK from Gram negative pathogens such as *Pseudomonas aeruginosa*[7] and the malaria parasite *Plasmodium falciparum*[8] reinforces the potential of the target across a variety of pathogens.

To the best of our knowledge, all of the Mtb TMK inhibitors reported so far either are thymidine monophosphate (TMP) analogs[9] or contain a thymidine core.[10] This is attributable to

Received: August 25, 2014
Published: December 8, 2014

DOI: 10.1021/jm5012947
J. Med. Chem. 2015, 58, 753−766

the fact that these inhibitors used a thymidine or pyrimidinone core as a starting point. In order to identify novel leads that exploit active site regions that are not explored by TMP analogs, we invested in high throughput screening (HTS) and fragment based lead generation (FBLG) approaches against Mtb TMK. Our objective was to achieve improved potency against the enzyme that would translate to cellular activity against mycobacteria (minimum inhibitory concentration, Mtb MIC). This has been one of the major challenges for lead generation against Mtb. Our efforts resulted in the identification of two novel classes of Mtb TMK inhibitors, 3-cyanopyridones and 1,6-naphthyridin-2-ones. Herein, we discuss the structure guided optimization of these two series and their potential as anti-TB agents. To the best of our knowledge, this is the first report of bona fide Mtb TMK inhibitors with non-thymidine cores.

RESULTS AND DISCUSSION

High-Throughput Screening Identifies 3-Cyanopyridones as Inhibitors of Mtb TMK. SiteMap[11] analyses of Mtb TMK suggest that the TMP site is highly druggable (Supporting Information S1). This was reflected in the high hit rate observed from an HTS of 120 000 compounds, a representative set of our corporate collection. Multiple leadlike scaffolds were obtained with activity in the range of 1−30 μM. Protein observed NMR studies confirmed the binding of the inhibitors to the TMP site. On the basis of potency, preliminary SAR from analog screening, and opportunity to diversify the scaffold, we prioritized the 3-cyanopyridone series for our hit to lead campaign (Figure 1). The ligand efficiency (LE = 0.46)[12,13] and lipophilic ligand efficiency (LLE = 3.54)[12,13] for compound **1**, our chosen starting point, suggested that the series is leadlike and suitable for further optimization.

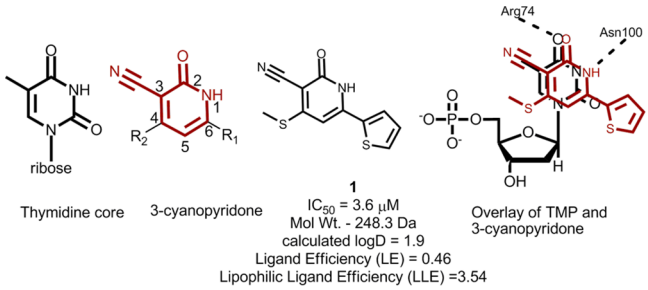

Figure 1. 3-Cyanopyridone scaffold identified as a hit from an HTS: 2D-overlay of TMP (black) and compound **1** (red) based on the predicted docking pose. The key H-bonding interactions are with Arg74 and Asn100.

In the early stage of the program, publicly available complex crystal structures of Mtb TMK with TMP analog azido TMP(AZT) (PDB code 1W2H)[5b] were used for modeling to understand the possible binding mode of the cyanopyridones. The carbonyl oxygen and NH of the pyridone ring form the key hydrogen bonding contact, interacting with the sidechains of Asn100 and Arg74 of Mtb TMK, whereas the pyridone ring makes a $\pi-\pi$ stacking interaction with Phe70 (Supporting Information S2, Figure S2-1A). An overlay with bound TMP indicated that the R_1 aryl ring aligns with the C2 carbonyl of TMP (Figure 1). Thus, this non-thymidine-like core gave access to a novel diversification point. We utilized this knowledge in our design and were able to reach submicromolar potency within 10 molecules from the starting hit (Table 1, compound **8**). The predicted binding mode was later confirmed by cocrystallization of cyanopyridone (**8**) with Mtb TMK. Features of the Mtb TMK TMP binding site and differentiation with respect to other bacterial TMKs and human TMK are discussed in the following sections.

Table 1. SAR Exploration of 3-Cyanopyridones

No	R_1	IC_{50} (μM)	Calculated logD	No.	R_2	IC_{50} (μM)	Calculated logD
1		3.6	1.9	**8**		0.42	0.2
2		1.9	2.0	**9**		2.73	0.25
3		1.9	2.7	**10**		1.01	2.5
4		>50	1.9	**11**		1.2	2.3
5		1.5	2.2	**12**	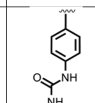	0.25	3.1
6		7.7	2.2	**13**		2.63	2.4
7		18.0	1.1	**14**	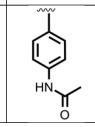	0.43	2.8

Key derivatives that helped in understanding the structure−activity relationship (SAR) for this series are shown in Table 1. Several aryl and heteroaryl groups at R_1 were tried (**1**−**7**, Table 1) among which we found 3-methoxyphenyl as the preferred group with an IC_{50} of 1.5 μM (**5**). Keeping the 3-methoxyphenyl at R_1 fixed, we next explored substituted aryl rings at R_2 (**8**−**14**). Aromatic rings at R_2 showed promising results, and a limited exploration of smaller substituents on the R_2 aryl ring resulted in several compounds with submicromolar potency. Para substituted derivatives such as the carboxylic acid, urea, and amide (**8**, **12**, and **14**, Table 1) were generally more potent.

While both pyridone and pyrimidinone cores (matched pair, **5**/**15**, Table 1 and Figure 2) were active, pyridones were found to be more potent. Similarly, replacement of pyridone with pyranone (matched pair, **1**/**16**, Table 1 and Figure 2) led to complete loss of activity against Mtb TMK. Replacement of cyano with other groups such as amide (matched pair, **3**/**17**, Table 1 and Figure 2) and methyl (matched pair, **8**/**18**, Table 1 and Figure 2) produced less potent or inactive compounds.

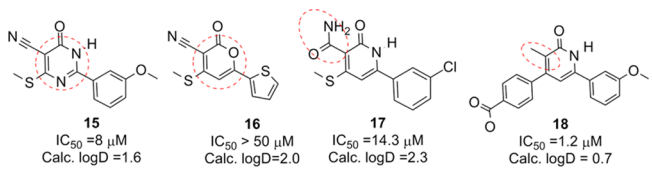

Figure 2. Limited SAR exploration of core ring and nitrile replacement.

DOI: 10.1021/jm5012947
J. Med. Chem. 2015, 58, 753−766

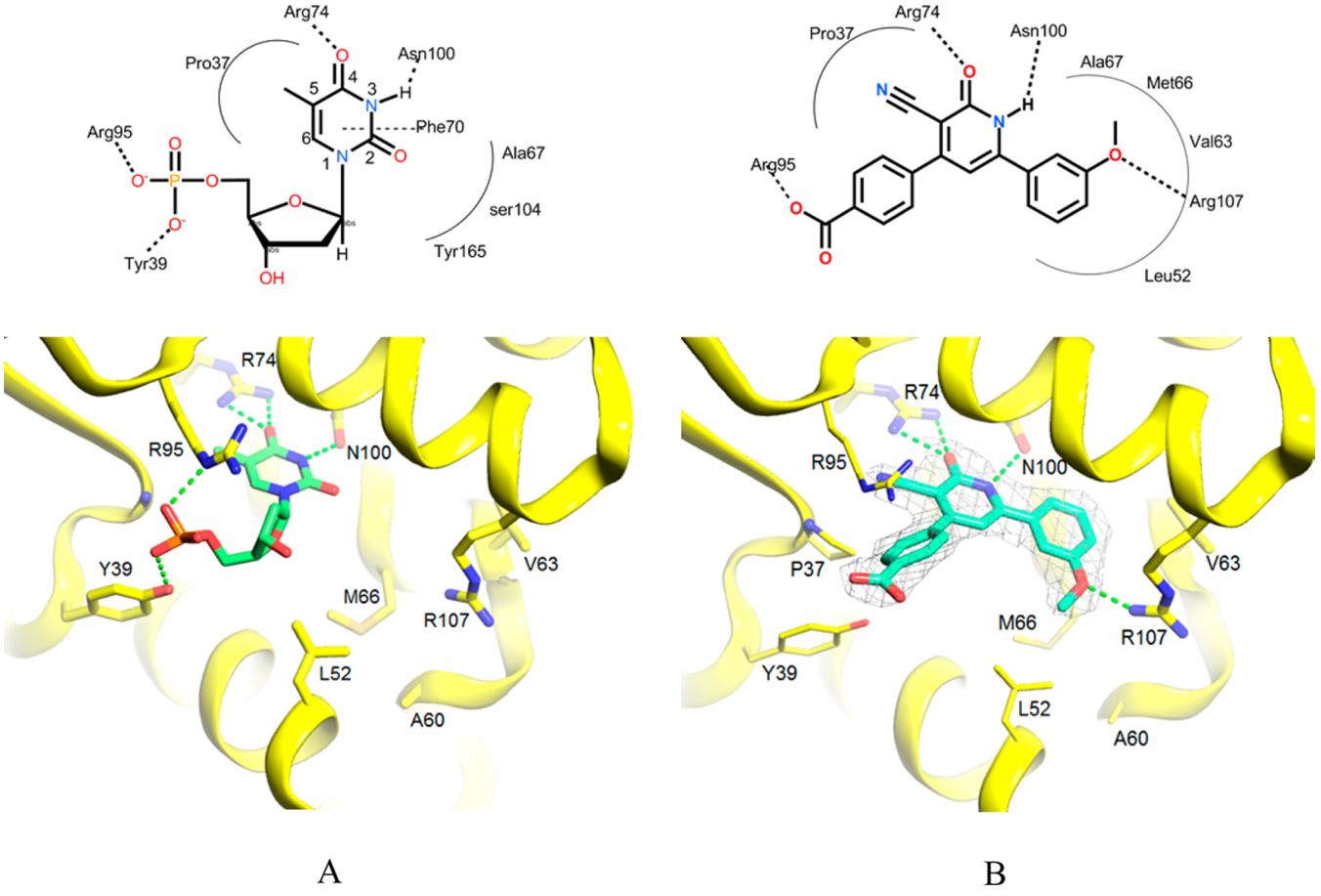

Figure 3. Crystal structures of Mtb TMK in complex with TMP[5a] (A, PDB code 1G3U) and compound **8** (B, 2.5 Å resolution): (A) key interactions exhibited by TMP; (B) key interactions made by compound **8** (PDB code 4UNN). Figures were prepared using PyMol, version 1.2. Protein is shown in yellow cartoon representation with selected side chains labeled and shown as sticks with carbon atoms colored yellow. Bound ligand is drawn in stick representation with carbon atoms in green (TMP) or cyan (compound **8**). H-bond interactions are shown as dotted green lines. Electron density for compound **8** is contoured at 1.0σ using $2f_o f_c$ coefficients and is displayed as a gray mesh.

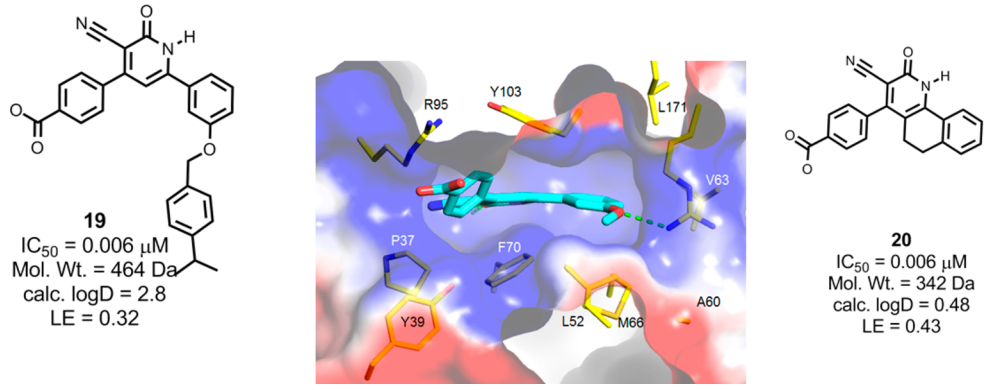

Figure 4. Molecular surface for the active site of Mtb TMK in complex with **8**. The color of the surface indicates the nature of the active site, where red and blue are hydrophilic areas and gray is the hydrophobic surface. Shown are structure and potency of compounds **19** and **20**.

This can be attributed to the electron withdrawing nature of the nitrile group which makes the pyridine ring electron deficient and thus strengthens the H-bonds between the pyridone carbonyl and NH, and the protein. Furthermore, modeling suggested that the nitrile group may be involved in a favorable dipolar contact with the side chain of Arg74.

Crystal Structures of Mtb TMK in Complex with 3-Cyanopyridones Rationalize SAR and Drive Improvements in Potency. We solved the crystal structure of the complex of Mtb TMK with compound **8** (Figure 3) and were gratified to note that the binding mode predicted from docking was in agreement with the crystallographic pose to within 1.0 Å RMSD (Supporting Information S2, Figure S2-1B). Figure 3A and Figure 3B show the key interactions of TMP and **8** in the Mtb TMK active site. The $\pi-\pi$ stacking of the pyridone ring with Phe70 and the interactions of the NH and C═O of the pyridone ring with Asn100 and Arg74 side chains, respectively, are the key interactions for both compounds. The nitrile group,

DOI: 10.1021/jm5012947
J. Med. Chem. 2015, 58, 753−766

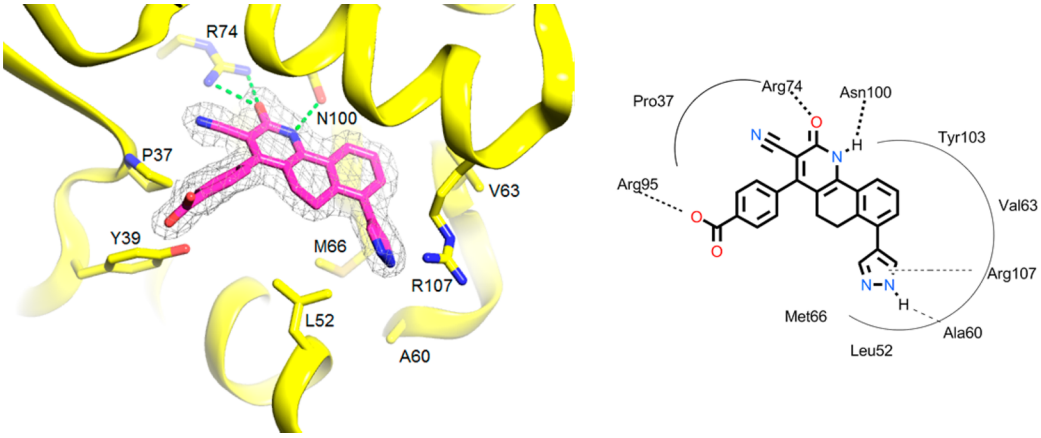

Figure 5. Cocrystal structure at 2.0 Å resolution of compound **23** with Mtb TMK (PDB code 4UNR). Protein is shown in yellow cartoon representation with selected side chains labeled and shown as sticks with carbon atoms colored yellow. Bound ligand is drawn in stick representation with carbon atoms in magenta. H-bond interactions are shown as dotted green lines. Electron density for compound **23** is contoured at 1.0σ using $2f_o f_c$ coefficients and is displayed as a gray mesh.

while not making an ideal hydrogen bond, is close to the side chain of Arg74 and is involved in favorable polar contacts with this residue. The hydrophobic pocket into which the methoxyphenyl projects and that comprises the side chains of Leu52, Ala53, Val63, Met66, Ala67, Phe70, Tyr165, and Leu171 is unique to the Mtb TMK active site. This is an important factor in the search for selective inhibitors. The para-benzoic acid at R_2 makes critical interactions with Arg95. In addition to a salt bridge between the carboxylate anion and the guanidine cation, the aromatic ring stacks against the π-system of the Arg95 side chain. This interaction may be responsible for the marked improvement in potency observed for cyanopyridones carrying this substituent.

Further analysis of the cocrystal structure of Mtb TMK with **8** suggested that the aforementioned hydrophobic pocket could be exploited to improve the potency (Figure 4). Of several medicinal chemistry designs investigated, two ideas led to single digit nanomolar potency. First, extension of the OMe group of **8** using a larger hydrophobic group (**19**) resulted in dramatic improvement in IC_{50}. Second, the torsion angle between the pyridone ring and the phenyl ring at R_1 in the cocrystal structure was noted to be 18°. Thus, introduction of an ethylene bridge between the two rings, and hence conformationally locking the rings, was predicted to lead to an improvement in potency due to a reduction in the entropic penalty combined with additional hydrophobic contacts with the ethylene group. This design led to compound **20**, a fused cyanopyridone, which showed a similar leap in potency as seen for **19** and had excellent ligand efficiency (Figure 4). Hence, we focused on the exploration of fused cyanopyridones as a means to overcoming one of the major challenges for bacterial TMK inhibitors, that of translating enzymatic activity into cellular activity.

We were successful in obtaining a cocrystal structure of the fused cyanopyridone, **23**, with Mtb TMK which indicated that this subseries holds promise to drive the potency further to the picomolar range likely required for adequate cellular activity (Figure 5). The position, orientation, and interactions of the core ring and substituents at R_1 and R_2 are similar to those observed for the open form of the cyanopyridone as predicted. The improvement in potency observed for the fused cyanopyridones can, therefore, be attributed to optimal interaction with the hydrophobic pocket and entropic advantage from the conformationally locked system.

A limited set of substituents were tested at R_1 to explore the possibility of picking up interactions with residues such as Ala60, Val63, and Arg107 (Table 2). The complex crystal structure of Mtb TMK with compound **23** suggests that the pyrazole ring NH forms an H-bond with the backbone carbonyl of Ala60. Compound **24**, a fused cyanopyridone with a longer aryl ether substituent at R_1, was the most potent compound in the series. This suggests that hybridization of designs based on

Table 2. SAR Exploration for Fused Cyanopyridones

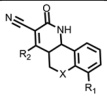

No	R_1	R_2	X	IC50 (μM)	Mtb MIC (μg/mL)	Calculated logD	pKa (Acid)
21	OH		C	0.003	> 32	0.2	4.4
22	OCH_3		C	0.005	> 32	0.27	4.4
23			C	0.002	> 32	0.36	4.4
24	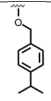		C	0.001	> 32	2.9	4.4
25	OCH_3	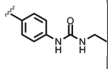	C	0.017	> 32	3.0	neutral
26	H	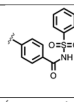	O	0.002	> 32	0.11	5.0
27	H		O	0.005	> 32	-1.06	3.9

DOI: 10.1021/jm5012947
J. Med. Chem. 2015, 58, 753−766

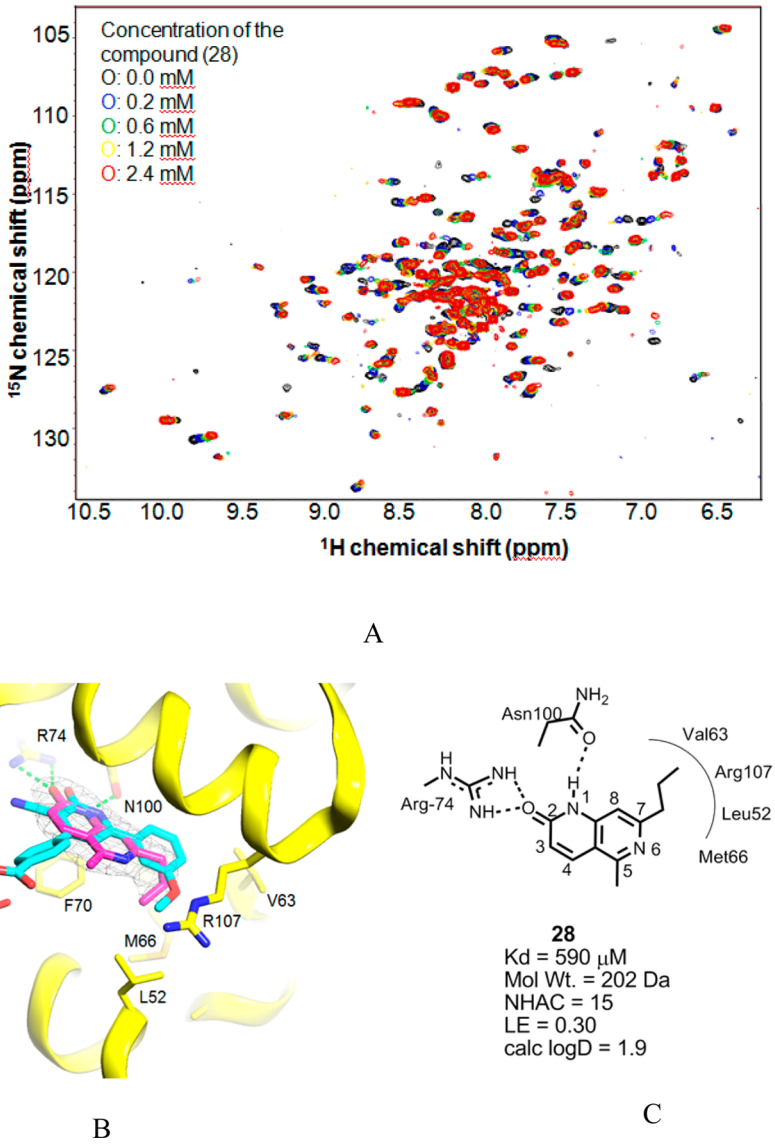

Figure 6. Identification of 1, 6-naphthyridinone fragment hit, **28**, from NMR based fragment screening. (A) Overlaid 2D NMR spectra showing the chemical shift perturbation at 0.2, 0.6, 1.2, and 2.4 mM compound **28**. (B) Crystal structure at 2.3 Å resolution showing the binding of FRIT **28** drawn in stick representation with carbon atoms in magenta in the TMP site of Mtb TMK (PDB code 4UNP). The crystallographic pose of cyanopyridone (**8**, cyan) has been overlaid for comparison. Protein from 4UNP is shown in yellow cartoon representation with selected side chains labeled and shown as sticks with carbon atoms colored yellow. H-bond interactions for **28** with the protein are shown as dotted green lines. Electron density for compound **28** is contoured at 1.0σ using $2f_o f_c$ coefficients and is displayed as a gray mesh. (C) 2D-interaction diagram. NHAC = number of heavy atom counts. LE = ligand efficiency.

the limited SAR obtained for compounds **19** and **20** is a promising approach and can be further exploited to optimize this series.

Despite high in vitro enzyme potency, the fused cyanopyridones did not exhibit any cellular activity even at the highest concentration tested in an Mtb whole cell assay (Mtb MIC > 32 μg/mL) (Table 2). We hypothesize that poor cellular permeability could be one of the reasons for the lack of Mtb MIC, and the ionic nature of the compounds (**21**−**24**, carboxylic acids) may be responsible for this. Thus, compounds with varying pK_a such as acyl sulfonamides, ureas, and amides (**25**−**27**) were synthesized and tested. Unfortunately, these compounds also failed to show any inhibition in a whole cell assay (Mtb MIC > 32 μg/mL) despite their potent enzymatic activity.

Fragment Based Lead Generation Identifies Alternative Core Scaffolds. In our pursuit of alternative cores and novel scaffolds with the potential for cellular activity, we screened a fragment library against Mtb TMK using a 2D-TROSY based NMR method. A set of 1200 fragments was screened in mixtures of 6. Hit mixtures were deconvoluted and the K_d values of the individual hits determined. This effort led to the identification of multiple fragment hits (FRITs) with LE of 0.25 or above. We generated cocrystal structures of a subset of the FRITs with Mtb TMK in order to understand their binding modes. In combination with the IC_{50} of close analogs this allowed us to understand the FRIT SAR and prioritize scaffolds for FRIT to hit optimization.

1,6-Naphthyridin-2-one (**28**, Figure 6B) was one of the most promising scaffolds resulting from this campaign. The chemical

DOI: 10.1021/jm5012947
J. Med. Chem. 2015, 58, 753−766

shifts observed when this ligand binds to Mtb TMK are shown in Figure 6A.

To gain insight into the FRIT binding mode, 1,6-naphthyridinone, **28**, was cocrystallized with Mtb TMK (Figure 6B and Figure 6C). The carbonyl oxygen and NH hydrogen of the naphthyridinone ring make the critical hydrogen bond contacts with Arg74 and Asn100, respectively. The naphthyridinone ring is involved in a $\pi-\pi$ stacking interaction with Phe70. An overlay with TMP and the cyanopyridone, **8**, indicated that the C-4 and C-7 positions of the ring can be exploited for further expansion.

We used the knowledge from this cocrystal structure, combined with the cocrystal structures and SAR for the cyanopyridone series, for the FRIT expansion campaign based on 1,6-naphthyridinone, **28**. A virtual library was designed via enumeration with suitable substituents at R_1 and R_2. The predicted binding modes of the virtual library and synthetic feasibility were used to prioritize compounds for synthesis. Encouragingly, we could achieve submicromolar potency for the 1,6-naphthyridinone series together with improved ligand efficiency with a limited set of compounds (Table 3).

Table 3. SAR Exploration for 1,6-Naphthyridinone

Compound #	Structure	IC_{50} (μM)	Ligand Efficiency (LE)	Calculated logD
29	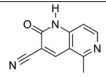	634	0.31	0.8
30	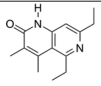	133	0.31	2.4
31	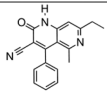	0.35	0.40	2.8
32	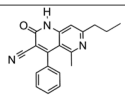	1.0	0.36	3.3
33	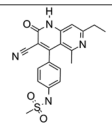	0.2	0.34	1.9
34	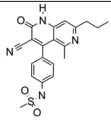	2.1	0.28	2.4

Compound **33**, the most potent in the series, was successfully cocrystallized with Mtb TMK (Figure 7). The position, orientation, and key interactions of the core ring were retained with respect to the starting FRIT, **28**. The aryl substituent at C-4 of the napthyridinone extends into the ribose and phosphate binding region, where it makes a number of new polar contacts. The NH of the sulfonamide group makes a hydrogen bond interaction with Asp9. The oxygen atoms of the sulfonamide group make water-mediated interactions with Tyr39 and Arg95. The ring nitrogen (6-aza) is involved in a water-mediated hydrogen bond with Arg107.

Exploration of substitution at C-7 indicated that an ethyl group is optimal (Table 3). Further extension led to a drop in potency (matched pairs **31**/**32** and **33**/**34**). Overlay of the docking poses of these matched pairs in the TMP binding site (not shown) showed a shift of the core ring for propyl derivatives so as to better accommodate the propyl group which clashes with residues in the hydrophobic pocket. Overlay of the complex crystal structures of compound **28** (propyl group at C-7) and compound **33** (ethyl group at C-7) confirmed the docking based predictions (Supporting Information S2, Figure S2-2), thus explaining the observed drop in potency upon homologation at this position. The relatively potent compounds (**31**−**34**, Table 3) when tested in the whole cell assay did not exhibit any activity (Mtb MIC > 32 μg/mL).

Thus, our FBLG campaign, with the application of limited synthetic chemistry, was able to deliver a novel chemical class, the 1,6-naphthyridinones, that shows submicromolar potency and improved ligand efficiency (0.35−0.40). However, further exploration is required to improve the potency and establish the potential of this chemical class as an antitubercular agent. The observed SAR and experimental binding modes lay the foundation for further investment in this series. For example, probing the C-5 and C-7 diversification points of the naphthyridinone ring so as to optimize the hydrophobic contacts in the unique hydrophobic pocket of Mtb TMK may lead to improvements in potency. Furthermore, substitution at the para position of the phenyl at C-4 can be further extended by applying the SAR knowledge from the cyanopyridones. No further work was done on the 1,6-naphthyridinone series as our focus shifted to the cyanopyridones which were in an advanced stage of lead generation.

Sulfoxide and Sulfone Subseries of the Cynanopyridones Exhibit Mtb MIC. During the course of initial exploration of SAR at the R_1 and R_2 positions of the 3-cyanopyridone ring, we found that the oxidized form of compound **1**, the sulfoxide **35**, exhibited moderate Mtb MIC (12 μg/mL, Table 4). This encouraged us to investigate this subseries further. We synthesized and tested a selected set of sulfoxides (**36**, **37**, **39**, and **41**) and sulfones (**38** and **40**). Our SAR knowledge from earlier exploration of the cyanopyridones was used to select appropriate R_1 substituents. We were encouraged to see that both sulfoxide and sulfone subseries of the cyanopyridones exhibited cellular activity and that the Mtb MIC improved concurrently with optimization of the IC_{50} against Mtb TMK (Table 4). Extension of the aryl ring at position R_1, in a similar manner to compound **19**, led to a 10-fold improvement in Mtb TMK IC_{50} (**40** and **41**) with retention of Mtb MIC. The sulfone **42**, which lacks the critical nitrile group, did not show any inhibition in our biochemical assay up to 25 μM and thus, unsurprisingly, had no measurable Mtb MIC (>32 μg/mL). In contrast to the equivalent aryl derivatives, compound **43**, the sulfone derivative of the fused cyanopyridone, exhibits weak activity against the enzyme (Table 2). Overall, we noted a reasonable correlation between IC_{50} and MIC within our limited data set, suggesting an on-target basis for the observed Mtb MIC.

In order to understand the mode of binding of this subseries, we cocrystallized compound **36** with Mtb TMK. Our structure revealed that the sulfoxide subseries binds in a similar manner as observed for other cyanopyridones (Figure 8). The sulfoxide moiety lies adjacent to the guanidine moiety of Arg95, suggesting they may form a cation/dipole interaction.

The observed correlation between Mtb TMK IC_{50} and Mtb MIC, in conjunction with confirmation of Mtb TMK binding in the form of complex crystal structures, is indicative of target

DOI: 10.1021/jm5012947
J. Med. Chem. 2015, 58, 753−766

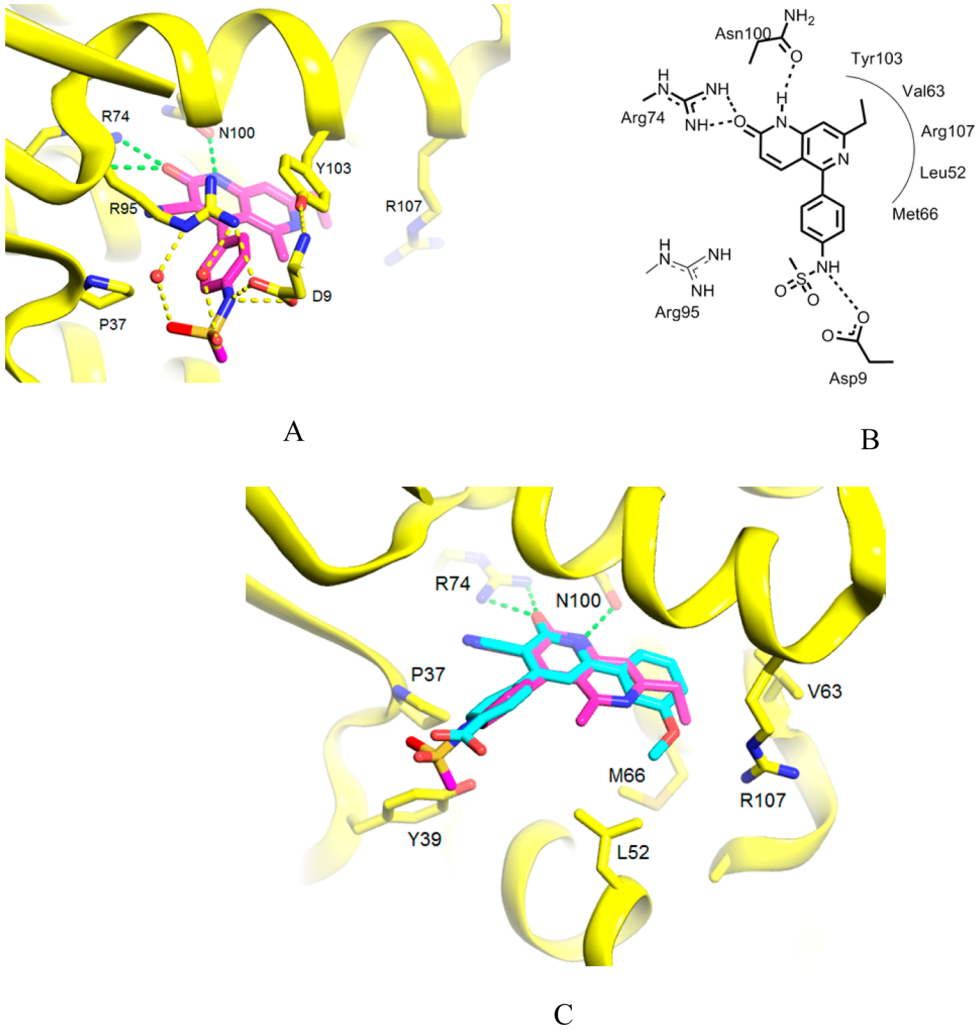

Figure 7. (A) Cocrystal structure at 2.2 Å resolution of compound **33** with Mtb TMK (PDB code 4UNS). (B) 2D-interaction diagram. Protein is shown in yellow cartoon representation with selected side chains labeled and shown as sticks with carbon atoms colored yellow. Bound ligand is drawn in stick representation with carbon atoms in magenta. H-bond interactions are shown as dotted green and yellow lines. Electron density for compound **3** is contoured at 1.0σ using $2f_o f_c$ coefficients and is displayed as a gray mesh. (C) Overlay of bound ligands and active site residues from cocrystal structures of Mtb TMK with cyanopyridone (**8**, cyan) and 1,6-naphthyridinone (**33**, magenta).

engagement. Further mode of action studies including resistance mutation mapping would be required to fully establish the target link.

Comparison of all the cyanopyridone subseries indicated that sulfoxides and sulfones may possess suitable physicochemical properties for further exploration so as to improve their antimicrobial activity against Mtb. Some of the differentiating properties associated with sulfoxides and sulfones are ionic nature (sulfone/sulfoxide are neutral; the potent aryl substutited pyridones in Tables 1 and 2 are mostly acidic), with pK_a of pyridone NH (calculated pK_a values are 6−7 for sulfones/sulfoxides, whereas for the aryl substituted derivatives the values are in the range 8−9; Supporting Information S3, Table S3-1). Further investigation such as experimental measurement of pK_a and design of neutral cyanopyridone derivatives with the desired pK_a is required to establish this hypothesis.

Inhibitor Selectivity: Comparison of the TMP Binding Sites in Mtb, Human, and Bacterial TMKs. Comparison of the Mtb TMK TMP binding site with that from other bacterial TMKs and human TMK revealed key differences in the active site (Supporting Information, S4, Figure S4-1 and Table S4-1). An overlay of the human TMK-TMP and Mtb TMK-compound **8** crystal structures shows that the aryl ring at R_1 of the cyanopyridone core may not be tolerated in human TMK (Figure 9). The methoxy substituted phenyl ring of **8** cannot be accommodated within the human TMK active site without a change in either the binding mode or the protein conformation (Figure 9). Residues in human TMK such as Thr106, Lys109, and Tyr151 would clash with the methoxy phenyl ring of **8**, suggesting that similarly substituted cyanopyridones will not inhibit human TMK.

Selected potent cyanopyridones (**5**, **12**, **21**, **27**, and **36**) were tested in a human TMK enzyme assay to confirm the structure-based prediction. None of the compounds showed any activity up to 200 μM (Supporting Information, Table S4-1), the highest concentration tested that confirmed the selectivity of cyanopyridones and the unique nature of Mtb TMK active site. A similar comparison of Mtb TMK with the TMP binding sites of other bacterial TMKs (*E. coli*, *S. aureus*, and *H. influenzae*) indicated that the cyanopyridones are likely to be selective for Mtb TMK (Supporting Information S4, Figure S4-1 and Table S4-1). This prediction was supported by IC_{50} data against other

DOI: 10.1021/jm5012947
J. Med. Chem. 2015, 58, 753−766

Table 4. Limited SAR Exploration of Sulfoxides and Sulfones

No	Structure	IC_{50} (μM)	Mtb MIC (μg/mL)	Calculated logD
35	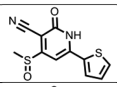	0.82	12	0.3
36	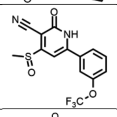	0.24	8	1.6
37	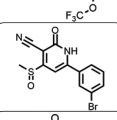	0.14	4	1.2
38	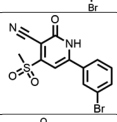	0.1	8	1.2
39	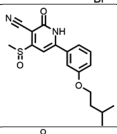	0.33	4	2.0
40	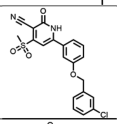	0.022	4	2.6
41	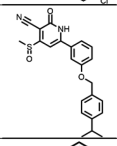	0.032	2	3.1
42	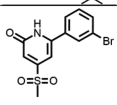	>25	>32	1.4
43	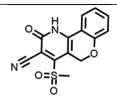	30	32	0.2

bacterial TMKs obtained for selected compounds from the series (Supporting Information S5, Figure S5-1).

The aforesaid results from our hit to lead for cyanopyridones and limited exploration of 1,6-naphthyridinones and selectivity against human TMK and other bacterial TMK clearly demonstrated that the development of selective and potent inhibitors against Mtb TMK is achievable. The antimycobacterial activity exhibited by sulfone and sulfoxides subseries (Table 4) was promising and indicated that modulation of physicochemical properties is vital in conjunction with potency against Mtb TMK to achieve cellular activity.

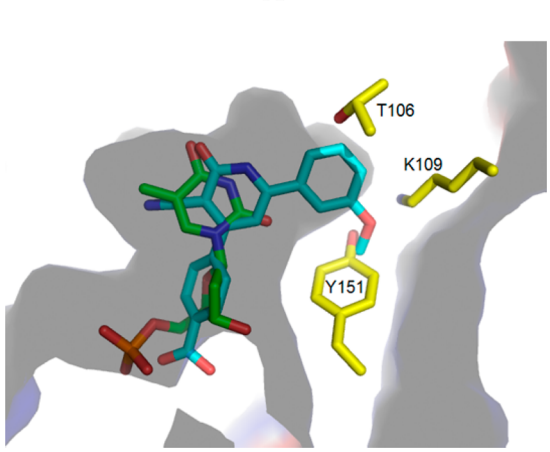

Figure 9. Comparison of the TMP binding sites of human and Mtb TMK. (A) Molecular surface of the TMP binding site of human TMK (PDB code 1E2D) is shown in gray. The binding mode of compound **8** (cyan carbon atoms) in Mtb TMK is overlaid with TMP (green carbon atoms) using protein atoms of the respective protein complexes (selected human TMK residues are colored yellow and labeled).

CONCLUSION

High throughput screening and fragment based lead generation approaches against Mtb TMK resulted in two novel chemical series, 3-cyanopyridone and 1,6-naphthyridinone, respectively. Structure guided optimization of the 3-cyanopyridone hit, **1**, led to compounds with single digit nanomolar potency in vitro, albeit devoid of any cellular activity. Interestingly, a subseries containing sulfoxide or sulfone substituents showed low micromolar Mtb MIC. While the IC_{50}–MIC correlation indicates that Mtb TMK may be one of the targets responsible for the observed cellular activity, the target link remains to be conclusively established. The 1,6-naphthyridin-2-ones were optimized to submicomolar potency within a limited number

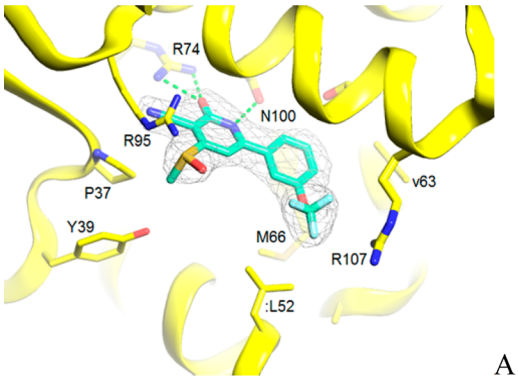

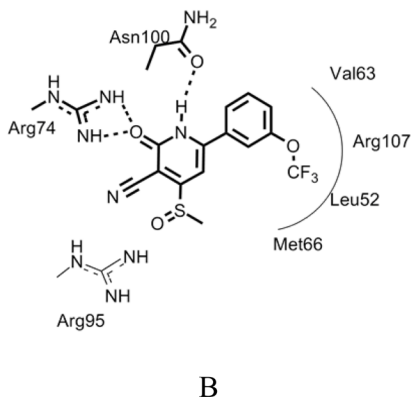

Figure 8. Cocrystal structure at 2.3 Å resolution of compound **36** with Mtb TMK (PDB code 4UNQ). (B) 2D-interaction diagram. Protein is shown in yellow cartoon representation with selected side chains labeled and shown as sticks with carbon atoms colored yellow. Bound ligand is drawn in stick representation with carbon atoms in cyan. H-bond interactions are shown as dotted green lines. Electron density for compound **36** is contoured at 1.0σ using $2f_o f_c$ coefficients and is displayed as a gray mesh.

DOI: 10.1021/jm5012947
J. Med. Chem. 2015, 58, 753−766

Scheme 1[a]

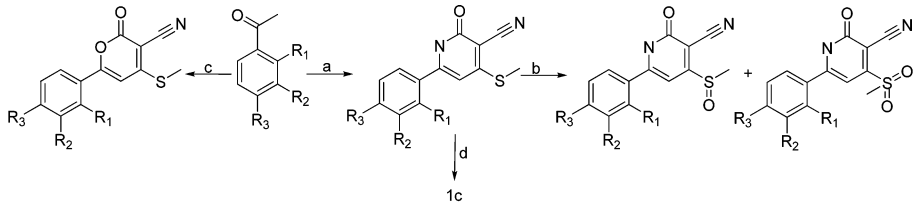

R_1, R_2= H, CH_3, OCH_3, Cl

R_3= OCH_3, 4-isopropylbenzyloxy, isopentyloxy, 3-chlorobenzyloxy, trifluoromethoxy

[a]Reagents and conditions: (a) 2-cyano-3,3-bis(methylthio)acrylamide, NaOH, DMSO, rt; (b) potassium monopersulfate triple salt, NMP, rt, 12 h; (c) 2-cyano-3,3-bis(methylthio)acrylate, NaOH, DMSO, rt; (d) dilute H_2SO_4, 50 °C, 4 h.

Scheme 2[a]

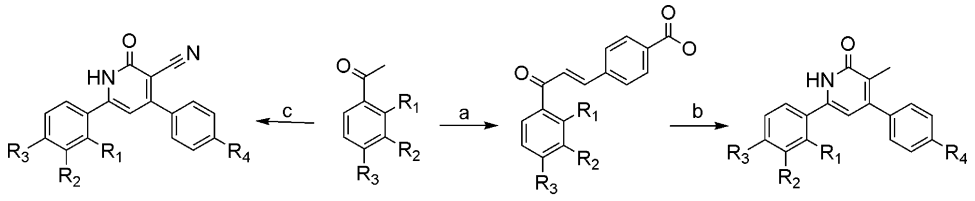

R_1, R_2= H, CH_3, OCH_3, Cl

R_3= OCH_3, 4-isopropylbenzyloxy

R_4= COOH, $COOCH_3$, NH_2, Urea, Amide, Sulphonamide, Acylsulphonamide

[a]Reagents and conditions: (a) aromatic aldehyde, NaOH, ethanol, rt, 3 h; (b) 2-(1*H*-benzo[*d*][1,2,3]triazol-1-yl)propanamide, NaOH, ethanol, reflux, 12 h; (c) aromatic aldehyde, ethyl cyanoacetate, ammonium acetate, ethanol, reflux, 12 h.

of compounds using cocrystal structures and SAR from the earlier series. Comparison of the active sites of Mtb, human, and bacterial TMKs indicates that these two classes of inhibitor are likely to be selective toward Mtb TMK, in agreement with the limited biochemical selectivity assay data to date. The SAR for both series, combined with the insights obtained from complex crystal structures generated during this lead generation program, paves the way for further optimization of the cyanopyridone and 1,6-naphthyridinone series toward identification of a candidate drug for the treatment of tuberculosis.

EXPERIMENTAL SECTION

Chemistry. General Procedures for the Synthesis of Compounds in Table 1 (Scheme 1). To the solution containing the corresponding acetyl derivative (0.599 mL, 5.55 mmol) in DMSO (25 mL) were added 2-cyano-3,3-bis(methylthio)acrylamide (1044 mg, 5.55 mmol) and powdered NaOH (444 mg, 11 mmol). The resulting reaction mixture was stirred at room temperature for 12 h. After the completion of the reaction, the reaction mixture was poured into water and neutralized with aqueous 1 N hydrochloric acid. The solid obtained was filtered, washed with water, and dried.

The crude compound was purified by flash chromatography using silica gel and ethyl acetate/hexane as eluent to obtain the corresponding pyridones. Subsequently preparative HPLC was used to provide compounds with >95% purity.

Procedure for the Synthesis of Compound 16. To the solution containing the corresponding acetyl derivative (500 mg, 3.96 mmol) in DMSO (25 mL) were added 2-cyano-3,3-bis(methylthio)acrylate (861 mg, 3.96 mmol) and powdered NaOH (317 mg, 7.93 mmol). The resulting reaction mixture was stirred at room temperature overnight. After the completion of the reaction, the reaction mixture was poured into water and neutralized with aqueous 1 N hydrochloric acid. The solid obtained was filtered, washed with water, and dried.

The crude compound was purified by flash chromatography using silica gel and ethyl acetate/hexane as eluent to obtain 4-(methylthio)-2-oxo-6-(thiophen-2-yl)-2*H*-pyran-3-carbonitrile in 58% yield. Subsequently preparative HPLC was used to provide compounds with >95% purity.

General Procedures for the Synthesis of Compounds in Table 2 (Scheme 2). To the solution of 1-(3-methoxyphenyl)-ethanone (0.457 mL, 3.33 mmol) in ethanol (50 mL) were added the corresponding aromatic aldehyde (3.33 mmol), ethyl 2-cyanoacetate (377 mg, 3.33 mmol), and ammonium acetate (1283 mg, 16.65 mmol). The resulting reaction mixture was refluxed overnight.

After the completion of the reaction, volatiles were removed under high vacuum in a rotaevaporator. The residue so obtained was triturated with water, filtered, and dried.

The crude compound was purified by flash chromatography using silica gel and methanol/dichloromethane as eluent to obtain the corresponding pyridones. Subsequently preparative HPLC was used to provide compounds with >95% purity.

Procedure for the Synthesis of Compound 18. To a solution of (*E*)-4-(3-(3-methoxyphenyl)-3-oxoprop-1-enyl)benzoic acid (148 mg, 0.53 mmol) in ethanol (15 mL) were added 2-(1*H*-benzo[*d*]-[1,2,3]triazol-1-yl)propanamide (100 mg, 0.53 mmol) and NaOH (52.6 mg, 1.31 mmol). The resulting suspension was refluxed overnight. After the completion of the reaction, the reaction mixture was cooled and the solid filtered and washed thoroughly with water. The crude compound was purified by flash chromatography using silica gel and methanol/dichloromethane as eluent to obtain 4-(6-(3-

DOI: 10.1021/jm5012947
J. Med. Chem. 2015, 58, 753−766

Scheme 3[a]

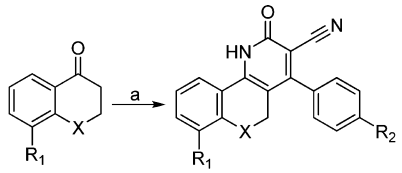

R_1= H, CH_3, OH, OCH_3, Pyrazole,4-isopropylbenzyloxy

X= C, O, N,

R_2=COOH, $COOCH_3$, NH_2, Urea, Amide, Sulphonamide, Acylsulphonamide

[a]Reagents and conditions: aromatic aldehyde, cyanoethyl acetate, NH_4OAc, reflux, overnight.

methoxyphenyl)-3-methyl-2-oxo-1,2-dihydropyridin-4-yl)benzoic acid in 25% yield.

Procedure for the Synthesis of 2-(1*H*-Benzo[*d*][1,2,3]triazol-1-yl)propanamide. To the reaction mixture containing sodium benzo[*d*][1,2,3]triazol-1-ide (2 g, 14.17 mmol) and 2-bromopropanamide (2.154 g, 14.17 mmol) in toluene (50 mL) was added 18-crown-6 (100 mg, 0.38 mmol). The reaction mixture was refluxed overnight. After the completion of the reaction, the reaction mixture was cooled and extracted with ethyl acetate. The ethyl acetate layer was washed with water and brine solution and dried over anhydrous sodium sulfate. The organic layer was evaporated at high vacuum. The solid obtained was taken for the next step without purification. The reaction mass, water, and the toluene layer were separated and evaporated to obtain 2-(1*H*-benzo[*d*][1,2,3]triazol-1-yl)propanamide in 74.2% yield. MS (ES+): m/z = 191 (M + H).

Procedure for the Synthesis of (*E*)-4-(3-(3-Methoxyphenyl)-3-oxoprop-1-enyl)benzoic Acid. To a solution of 1-(3-methoxyphenyl)ethanone (0.457 mL, 3.33 mmol) in ethanol (10 mL) were added 4-formylbenzoic acid (500 mg, 3.33 mmol) and sodium hydroxide (266 mg, 6.66 mmol). The reaction mixture was stirred at room temperature for 2 h. After the completion of the reaction, the volatiles were evaporated under vacuum. The solid obtained was taken up in water and neutralized cautiously to get the solid. The solid so obtained was filtered, washed with water, and dried. Yield: 53.2%. Subsequently preparative HPLC was used to provide compounds with >95% purity. MS (ES+): m/z = 282.9 (M + H).

General Procedures for the Synthesis of Compounds in Table 2 (21−25) (Scheme 3). To the corresponding 3,4-dihydronaphthalen-1(2*H*)-one (0.34 mmol) in ethanol (15 mL) were added the corresponding aldehyde (0.34 mmol), ethyl 2-cyanoacetate (0.34 mmol), and ammonium acetate (1.7 mmol). The resulting suspension was refluxed overnight. After the completion of the reaction, volatiles were evaporated and the residue so obtained was taken up in water, triturated, and filtered. The compound was purified by chromatography using silica gel and methanol/dichloromethane as eluent. Yield: 60−80%. Subsequently preparative HPLC was used to provide compounds with >95% purity.

General Procedures for the Synthesis of Compounds in Table 2 (26 and 27). To the corresponding chroman-4-one (1.73 mmol) in ethanol (15 mL) were added the corresponding aldehyde (1.73 mmol), ethyl 2-cyanoacetate (1.73 mmol), and ammonium acetate (8.64 mmol). The resulting suspension was refluxed overnight. After the completion of the reaction, volatiles were evaporated, the residue obtained was taken up in water, triturated, and filtered. The compound was purified by chromatography using silica gel and methanol/dichloromethane as eluent. Yield: 60−80%. Subsequently preparative HPLC was used to provide compounds with >95% purity.

General Procedures for the Synthesis of Compounds in Scheme 4. To the solution of cyanoacetic acid in ethyl acetate was added T3P and triethylamine. The reaction mass was stirred at room temperature for 10 min. Compound i was added and heated at 110 °C

Scheme 4. [a]: Synthesis of 1,6-Naphthyridinones (Table 3, Compounds 31−34)

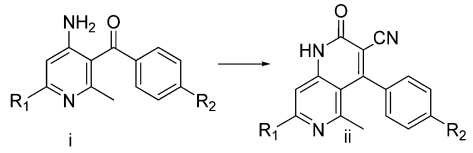

R_1=ethyl, propyl

R_2=H, Br, $NHSO_2CH_3$

[a]Reagents and conditions: cyanoacetic acid (6 equiv), T3P (20 equiv), TEA (2 equiv), ethyl acetate (10 vol), 110 °C, overnight.

overnight. After completion of the reaction, the reaction mass was cooled to room temperature and partitioned between ethyl acetate and water. The organic layer was washed with water and brine solution. The organic layer was then dried over sodium sulfate and evaporated under high vacuum to obtain the crude compound, which upon purification by chromatography using silica gel and methanol/dichloromethane as eluent gave the compounds in 25−50% yield. Subsequently preparative HPLC was used to provide compounds with >95% purity.

The compounds **28**, **29**, and **30** were procured from AstraZeneca fragment repository, and purity of the samples was confirmed to be >95% based on standard analytical method. The syntheses of these fragments are reported in the literature.[14]

General Procedures for the Synthesis of Compounds in Table 4 (Compounds 35−43). To the solution of the corresponding 4-(methylthio)-2-oxo-1,2-dihydropyridine-3-carbonitrile (0.29 mmol) in NMP (10 mL) was added potassium monopersulfate triple salt (1763 mg, 2.87 mmol). The reaction mixture was stirred at room temperature overnight. Both sulfone and sulfoxide were formed in the reaction.

After completion, the reaction was poured into water. The solid obtained was filtered, washed with water, and dried. The crude solid was purified by chromatography using silica gel and ethyl acetate/hexane as eluent to isolate the sulfoxide (yield, 10−30%) and sulfone (yield, 20−40%). Subsequently preparative HPLC was used to provide compounds with >95% purity.

4-(Methylthio)-2-oxo-6-(thiophen-2-yl)-1,2-dihydropyridine-3-carbonitrile (1). ^{1}H NMR (300 MHz, DMSO-d_6) δ 2.70 (s, 3H), 6.65(s, 1H), 7.25−7.35(m, 1H), 7.95(dd, J = 2.17, 8.52 Hz, 1H), 8.05−8.15 (m, 1H), 12.50 (br, s, 1H). HRMS: m/z (ES+) 248.0078 (MH^+) for $C_{11}H_8N_2OS_2$.

4-(Methylthio)-2-oxo-6-phenyl-1,2-dihydropyridine-3-carbonitrile (2). ^{1}H NMR (300 MHz, DMSO-d_6) δ 2.70 (s, 3H), 6.60 (s,

DOI: 10.1021/jm5012947
J. Med. Chem. 2015, 58, 753−766

1H), 7.50−7.70 (m, 3H), 7.80−7.95 (m, 2H), 12.50 (br, s, 1H). HRMS: *m/z* (ES+) 243.0583 (MH^+) for $C_{13}H_{10}N_2OS$.

6-(3-Chlorophenyl)-4-(methylthio)-2-oxo-1,2-dihydropyridine-3-carbonitrile (3). ^{1}H NMR (300 MHz, DMSO-d_6) δ 2.45 (s, 3H), 6.60 (s, 1H), 7.12−7.18 (m, 1H), 7.38−7.42 (m, 3H),12.00 (br, s, 1H). HRMS: *m/z* (ES+) 276.0124 (MH^+) for $C_{13}H_9ClN_2OS$.

6-(2-Methoxyphenyl)-4-(methylthio)-2-oxo-1,2-dihydropyridine-3-carbonitrile (4). ^{1}H NMR (300 MHz, DMSO-d_6) δ 2.85 (s, 3H), 3.90 (s, 3H), 6.60 (s, 1H), 7.10−7.20 (m, 1H), 7.38−7.42 (m, 3H), 12.00 (br, s, 1H). HRMS: *m/z* (ES+) 273.0687 (MH^+) for $C_{14}H_{12}N_2O_2S$.

6-(3-Methoxyphenyl)-4-(methylthio)-2-oxo-1,2-dihydropyridine-3-carbonitrile (5). ^{1}H NMR (300 MHz, DMSO-d_6) δ 2.75 (s, 3H), 3.85 (s, 3H), 6.60 (s, 1H), 7.10−7.20 (m, 1H), 7.38−7.42 (m, 3H), 12.00 (br, s, 1H). HRMS: *m/z* (ES+) 273.0687 (MH^+) for $C_{14}H_{12}N_2O_2S$.

6-(4-Methoxyphenyl)-4-(methylthio)-2-oxo-1,2-dihydropyridine-3-carbonitrile (6). ^{1}H NMR (300 MHz, DMSO-d_6) δ 2.70 (s, 3H), 3.84 (s, 3H), 6.54 (s, 1H), 7.08 (d, *J* = 8.85 Hz, 2H), 7.84 (d, *J* = 8.85 Hz, 2H), 12.37 (br s, 1H). HRMS: *m/z* (ES+) 273.0686 (MH^+) for $C_{14}H_{12}N_2O_2S$.

4-(Methylthio)-2-oxo-6-(pyridin-2-yl)-1,2-dihydropyridine-3-carbonitrile (7). ^{1}H NMR (300 MHz, DMSO-d_6) δ 2.75 (s, 3H), 7.15 (s, 1H), 7.55−7.65 (m, 1H), 8.00−8.10 (m, 1H), 8.30 (d, *J* = 7.5 Hz, 1H), 8.75 (d, *J* = 4.5 Hz, 1H), 12.00 (s, 1H). HRMS: *m/z* (ES+) 244.0534 (MH^+) for $C_{12}H_9N_3OS$.

4-(3-Cyano-6-(3-methoxyphenyl)-2-oxo-1,2-dihydropyridin-4-yl)benzoic Acid (8). ^{1}H NMR (300 MHz, DMSO-d_6) δ 3.84 (s, 3H), 6.76−6.96 (m, 1H), 7.00−7.15 (m, 1H), 7.32−7.59 (m, 3H), 7.75 (d, *J* = 8.10 Hz, 2H), 8.05 (d, *J* = 8.29 Hz, 2H), 12.20 (s, 1H), 13.50 (br, s, 1H). HRMS: *m/z* (ES+) 347.0945 (MH^+) for $C_{20}H_{14}N_2O_4$.

3-(3-Cyano-6-(3-methoxyphenyl)-2-oxo-1,2-dihydropyridin-4-yl)benzoic Acid (9). ^{1}H NMR (300 MHz, DMSO-d_6) δ 3.79 (s, 3H), 6.53 (s, 1H), 6.94−7.07 (m, 1H), 7.32−7.41 (m, 3H), 7.52 (d, *J* = 8.29 Hz, 2H), 8.04 (d, *J* = 8.29 Hz, 2H), 11.71 (br, s, 1H), 12.70 (br, s, 1H). HRMS: *m/z* (ES+) 347.1025 (MH^+) for $C_{20}H_{14}N_2O_4$.

4-(4-Aminophenyl)-6-(3-methoxyphenyl)-2-oxo-1,2-dihydropyridine-3-carbonitrile (10). ^{1}H NMR (300 MHz, DMSO-d_6) δ 3.75 (s, 3H), 5.45 (br s, 2H), 6.69−6.76 (m, 2H), 6.80 (d, *J* = 8.10 Hz, 1H), 6.83−6.86 (m, 1H), 7.05−7.10 (m, 1H), 7.18 (t, *J* = 7.82 Hz, 1H), 7.39−7.45 (m, 3H), 12.48 (br s, 1H). HRMS: *m/z* (ES+) 318.1236 (MH^+) for $C_{19}H_{15}N_3O_2$.

4-(3-Aminophenyl)-6-(3-methoxyphenyl)-2-oxo-1,2-dihydropyridine-3-carbonitrile (11). ^{1}H NMR (300 MHz, DMSO-d_6) δ 3.85 (s, 3H), 5.34 (br s, 2H), 6.69−6.76 (m, 2H), 6.80 (d, *J* = 8.10 Hz, 1H), 6.83−6.86 (m, 1H), 7.07−7.14 (m, 1H), 7.18 (t, *J* = 7.82 Hz, 1H), 7.41−7.48 (m, 3H), 12.51 (br s, 1H). HRMS: *m/z* (ES+) 318.1236 (MH^+) for $C_{19}H_{15}N_3O_2$.

1-(4-(3-Cyano-6-(3-methoxyphenyl)-2-oxo-1,2-dihydropyridin-4-yl)phenyl)-3-ethylurea (12). ^{1}H NMR (300 MHz, DMSO-d_6) δ 1.05 (t, J = 12.5 Hz, 3H), 3.15 (q, *J* = 13.78, 2H), 3.85 (s, 3H), 6.25 (t, *J* = 10.5 Hz, 1H), 6.80 (br, s, 1H), 7.09−7.15 (m, 1H), 7.38−7.49 (m, 3H), 7.58 (d, *J* = 8.50 Hz, 2H), 7.68 (d, *J* = 8.50 Hz, 2H), 8.80 (s, 1H), 12.65 (br, s, 1H). HRMS: *m/z* (ES+) 389.1605 (MH^+) for $C_{22}H_{20}N_4O_3$.

6-(3-Methoxyphenyl)-2-oxo-4-(pyridin-3-yl)-1,2-dihydropyridin-3-carbonitrile (13). ^{1}H NMR (300 MHz, DMSO-d_6) δ 3.85 (s, 3H), 7.04−7.16 (m, 2H), 7.44 (s, 1H), 7.61 (dd, *J* = 4.71, 7.91 Hz, 2H), 8.18 (td, *J* = 1.95, 7.96 Hz, 1H), 8.50−8.64 (m, 1H), 8.76 (dd, *J* = 1.51, 4.90 Hz, 1H), 8.89−8.98 (m, 1H), 12.84 (br s, 1H). HRMS: *m/z* (ES+) 304.1075 (MH^+) for $C_{18}H_{13}N_3O_2$.

***N*-(4-(3-Cyno-6-(3-methoxyphenyl)-2-oxo-1,2-dihydropyridin-4-yl)phenyl)acetamide (14).** ^{1}H NMR (300 MHz, DMSO-d_6) δ 2.09 (s, 3H), 3.85 (s, 3H), 6.82 (br s, 1H), 7.12 (dd, *J* = 2.17, 9.32 Hz, 1H), 7.35−7.54 (m, 3H), 7.66−7.83 (m, 4H), 10.16−10.34 (m, 1H), 12.71 (br s, 1H). HRMS: *m/z* (ES+) 360.1259 (MH^+) for $C_{21}H_{17}N_3O_3$.

2-(3-Methoxyphenyl)-4-(methylthio)-6-oxo-1,6-dihydropyrimidine-5-carbonitrile (15). ^{1}H NMR (300 MHz, DMSO-d_6) δ 2.60 (s, 3H), 3.85 (s, 3H), 7.24 (dd, *J* = 2.45, 8.29 Hz, 1H), 7.50 (t, *J* = 8.01 Hz, 1H), 7.70−7.97 (m, 2H), 13.21 (br, s, 1H). HRMS: *m/z* (ES+) 273.0570 (MH^+) for $C_{13}H_{11}N_3O_2S$.

4-(Methylthio)-2-oxo-6-(thiophen-2-yl)-2*H*-pyran-3-carbonitrile (16). ^{1}H NMR (300 MHz, DMSO-d_6) δ 2.80 (s, 3H), 7.15 (s, 1H), 7.30−7.40 (m, 1H), 8.05 (dd, *J* = 2.17 Hz, 9.32 Hz, 1H), 8.15−8.22 (m, 1H). HRMS: *m/z* (ES+) 249.9990 (MH^+) for $C_{11}H_7NO_2S_2$.

6-(3-Chlorophenyl)-4-(methylthio)-2-oxo-1,2-dihydropyridine-3-carboxamide (17). ^{1}H NMR (300 MHz, DMSO-d_6) δ 2.45 (s, 3H), 6.60 (s, 1H), 7.28 (br, s, 1H), 7.50−7.67 (m, 2H), 7.79 (d, *J* = 7.5 Hz, 1H), 7.93 (s, 1H), 9.20 (br, s, 1H), 12.30 (br, s,1H). HRMS: *m/z* (ES+) 295.0297 (MH^+) for $C_{13}H_{11}ClN_2O_2S$.

4-(6-(3-Methoxyphenyl)-3-methyl-2-oxo-1,2-dihydropyridin-4-yl)benzoic Acid (18). ^{1}H NMR (300 MHz, DMSO-d_6) δ 1.97 (s, 3H), 3.89 (s, 3H), 6.53 (s, 1H), 6.94−7.07 (m, 1H), 7.32−7.41 (m, 3H), 7.52 (d, *J* = 8.29 Hz, 2H), 8.04 (d, *J* = 8.29 Hz, 2H), 11.71 (br s, 1H), 12.84 (br s, 1H). HRMS: *m/z* (ES+) 336.1157 (MH^+) for $C_{20}H_{17}NO_4$.

4-(3-Cyano-6-(3-(4-isopropylbenzyloxy)phenyl)-2-oxo-1,2-dihydropyridin-4-yl)benzoic Acid (19). ^{1}H NMR (300 MHz, DMSO-d_6) δ 1.20 (d, *J* = 6.97 Hz, 6H), 2.89 (td, *J* = 6.81, 13.70 Hz, 1H), 4.99−5.26 (m, 2H), 6.77−7.01 (m, 1H), 7.19 (d, *J* = 7.35 Hz, 1H), 7.27 (d, *J* = 8.10 Hz, 2H), 7.34−7.54 (m, 4H), 7.58 (br s, 1H), 7.85 (d, *J* = 8.10 Hz, 2H), 8.11 (d, *J* = 8.10 Hz, 2H), 12.91−13.23 (m, 2H). HRMS: *m/z* (ES+) 465.1736 (MH^+) for $C_{29}H_{24}N_2O_4$.

4-(3-Cyano-2-oxo-1,2,5,6-tetrahydrobenzo[h]quinolin-4-yl)-benzoic Acid (20). ^{1}H NMR (300 MHz, DMSO-d_6) δ 2.32 (t, *J* = 7.54 Hz, 2H), 2.67 (t, *J* = 7.54 Hz, 2H), 6.99 (d, *J* = 7.72 Hz, 1H), 7.21 (t, *J* = 8.01 Hz, 1H), 7.49−7.70 (m, 3H), 7.99−8.26 (m, 2H), 9.74 (br s, 1H), 12.63−13.28 (m, 2H). HRMS: *m/z* (ES+) 342.1004 (MH^+) for $C_{21}H_{14}N_2O_3$.

4-(3-Cyano-7-hydroxy-2-oxo-1,2,5,6-tetrahydrobenzo[*h*]-quinolin-4-yl)benzoic Acid (21). ^{1}H NMR (300 MHz, DMSO-d_6) δ 2.32 (t, *J* = 7.54 Hz, 2H), 2.67 (t, *J* = 7.54 Hz, 2H), 6.99 (d, *J* = 7.72 Hz, 1H), 7.21 (t, *J* = 8.01 Hz, 1H), 7.49−7.70 (m, 3H), 7.99−8.26 (m, 2H), 9.74 (br s, 1H), 12.63−13.28 (m, 2H). HRMS: *m/z* (ES+) 359.1025 (MH^+) for $C_{21}H_{17}N_2O_4$.

4-(3-Cyano-7-methoxy-2-oxo-1,2,5,6-tetrahydrobenzo[*h*]-quinolin-4-yl)benzoic Acid (22). ^{1}H NMR (300 MHz, DMSO-d_6) δ 2.32 (br s, 2H), 2.70 (t, *J* = 7.25 Hz, 2H), 3.82 (s, 3H), 7.17 (d, *J* = 8.29 Hz, 1H), 7.38 (t, *J* = 8.01 Hz, 1H), 7.57 (d, *J* = 8.29 Hz, 2H), 7.72 (d, *J* = 7.35 Hz, 1H), 8.10 (d, *J* = 8.29 Hz, 2H), 12.68 (s, 1H), 13.14 (br s, 1H). HRMS: *m/z* (ES+) 373.1095 (MH^+) for $C_{22}H_{16}N_2O_4$.

4-(3-Cyano-2-oxo-7-(1*H*-pyrazol-4-yl)-1,2,5,6-tetrahydrobnzo[*h*]quinolin-4-yl)benzoic acid (23). ^{1}H NMR (300 MHz, DMSO-d_6) δ 2.30 (t, *J* = 7.06 Hz, 2H), 2.78−2.93 (m, 2H), 7.33−7.48 (m, 1H), 7.54 (d, *J* = 8.29 Hz, 3H), 7.72−7.86 (m, 2H), 8.01 (d, *J* = 7.91 Hz, 1H), 8.09 (d, *J* = 8.10 Hz, 2H), 10.98−12.99 (m, 2H), 13.14 (br s, 1H). HRMS: *m/z* (ES+) 409.1352 (MH^+) for $C_{24}H_{16}N_4O_3$.

4-(3-Cyano-7,4-isopropylbenzyloxy)-2-oxo-1,2,5,6-tetrahydrobenzo[*h*]quinolin-4-yl)benzoic Acid (24). ^{1}H NMR (300 MHz, DMSO-d_6) δ 1.16−1.21 (m, 6H), 2.32 (br s, 2H), 2.67−2.80 (m, 2H), 2.81−2.96 (m, 1H), 5.13 (s, 2H), 7.20−7.29 (m, 3H), 7.35 (d, *J* = 7.72 Hz, 3H), 7.57 (d, *J* = 8.29 Hz, 2H), 7.73 (d, *J* = 8.10 Hz, 1H), 8.09 (d, *J* = 8.48 Hz, 2H), 12.05 (br s, 1H), 12.25 (br s, 1H). HRMS: *m/z* (ES+) 491.1985 (MH^+) for $C_{31}H_{26}N_2O_4$.

1-[4-(3-Cyano-7-methoxy-2-oxo-1,2,5,6-tetrahydrobenzo-[*h*]quinolin-4-yl)phenyl]-3-ethylurea (25). ^{1}H NMR (300 MHz, DMSO-d_6) δ 1.15 (t, *J* = 12.5 Hz, 3H), 2.30 (br s, 2H), 2.80 (br s, 2H), 3.20 (q, *J* = 13.78, 2H), 3.80 (s, 3H), 6.28 (t, *J* = 10.5 Hz, 1H), 6.80 (br, s, 1H), 7.09−7.15 (m, 1H), 7.38−7.49 (m, 2H), 7.60 (d, *J* = 8.50 Hz, 2H), 7.72 (d, *J* = 8.50 Hz, 2H), 12.65 (br, s, 1H). HRMS: *m/z* (ES+) 415.1692 (MH^+) for $C_{24}H_{22}N_4O_3$.

4-(3-Cyano-2-oxo-2,5-dihydro-1*H*-chromeno[4,3-*b*]pyridin-4-yl)-*N*-(phenylsulfonyl)benzamide (26). ^{1}H NMR (300 MHz, DMSO-d_6) δ 4.76 (br s, 2H), 6.97−7.09 (m, 1H), 7.17 (t, *J* = 7.63 Hz, 1H), 7.40−7.58 (m, 3H), 7.59−7.75 (m, 3H), 8.03 (t, *J* = 7.91 Hz, 4H), 8.12 (d, *J* = 7.35 Hz, 1H), 12.72 (br s, 1H), 12.94 (br s, 1H). HRMS: *m/z* (ES+) 484.0954 (MH^+) for $C_{26}H_{17}N_3O_5S$.

***N*-4-(3-Cyano-2-oxo-2,5-dihydro-1*H*-chromeno[4,3-*b*]-pyridin-4-yl)phenyl)methanesulfonamide (27).** ^{1}H NMR (300

DOI: 10.1021/jm5012947
J. Med. Chem. 2015, 58, 753−766

MHz, DMSO-d_6) δ 2.95 (s, 3H), 4.76 (br s, 2H), 6.97−7.09 (m, 1H), 7.17 (t, J = 7.63 Hz, 1H), 7.40−7.58 (m, 3H), 7.59−7.75 (m, 2H), 8.12 (d, J = 7.35 Hz, 1H), 12.72 (br s, 1H), 12.94 (br s, 1H). HRMS: m/z (ES+) 393.1654 (MH^+) for $C_{20}H_{15}N_3O_4S$.

7-Ethyl-5-methyl-2-oxo-4-phenyl-1,2-dihydro-1,6-naphthyridine-3-carbonitrile (31). ^{1}H NMR (300 MHz, DMSO-d_6) δ 1.21 (t, J = 7.54 Hz, 3H), 1.84 (s, 3H), 2.72 (q, J = 7.60 Hz, 2H), 7.10 (s, 1H), 7.35−7.42 (m, 2H), 7.52−7.65 (m, 3H), 12.69 (br s, 1H). HRMS: m/z (ES+) 290.12946 (MH^+) for $C_{18}H_{15}N_3O$.

5-Methyl-2-oxo-4-phenyl-7-propyl-1,2-dihydro-1,6-naphthyridine-3-carbonitrile (32). ^{1}H NMR (300 MHz, DMSO-d_6) δ 0.92 (t, J = 7.35 Hz, 3H), 1.55−1.73 (m, 2H), 1.84 (s, 3H), 2.67 (t, J = 7.44 Hz, 2H), 7.04 (s, 1H), 7.32−7.50 (m, 2H), 7.52−7.64 (m, 3H), 12.17 (brs, 1H). HRMS: m/z (ES+) 304.1371 (MH^+) for $C_{19}H_{17}N_3O$.

***N*-[4-(3-Cyano-7-ethyl-5-methyl-2-oxo-1,2-dihydro-1,6-naphthyridin-4-yl)phenyl]methanesulfonamide (33).** ^{1}H NMR (300 MHz, DMSO) δ 1.12−1.36 (m, 3H), 1.90 (s, 3H), 2.54 (s, 3H), 2.61−2.82 (m, 2H), 7.05 (s, 1H), 7.35−7.42 (m, 2H), 7.46−7.53 (m, 2H), 10.52 (s, 1H), 12.69 (br s, 1H). HRMS: m/z (ES+)383.1172 (MH^+) for $C_{19}H_{18}N_4O_3S$.

***N*-[4-(3-Cyano-7-propyl-5-methyl-2-oxo-1,2-dihydro-1,6-naphthyridin-4-yl)phenyl]methanesulfonamide (34).** ^{1}H NMR (300 MHz, DMSO-d_6) δ 0.92 (t, J = 7.35 Hz, 3H), 1.55−1.72 (m, 2H), 1.88 (s, 3H), 2.52 (s, 3H), 2.67 (t, J = 7.44 Hz, 2H), 7.02 (s, 1H), 7.38−7.42 (m, 2H), 7.48−7.53 (m, 2H), 10.45 (s, 1H), 12.50 (br s, 1H). HRMS: m/z (ES+) 397.1265 (MH^+) for $C_{20}H_{20}N_4O_3S$.

4-(Methylsulfinyl)-2-oxo-6-(thiophen-2-yl)-1,2-dihydropyridine-3-carbonitrile (35). ^{1}H NMR (300 MHz, DMSO-d_6) δ 2.97 (s, 3H), 7.21 (dd, J = 3.77, 5.09 Hz, 1H), 7.73 (d, J = 3.77 Hz, 1H), 7.91 (dd, J = 1.13, 5.09 Hz, 1H), 8.40 (s, 1H), 13.08 (br s, 1H). HRMS: m/z (ES+) 265.0031 (MH^+) for $C_{11}H_8N_2O_2S_2$.

4-(Methylsulfinyl)-2-oxo-6-(3-(trifluoromethoxy)phenyl)-1,2-dihydropyridine-3-carbonitrile (36). ^{1}H NMR (300 MHz, DMSO-d_6) δ 2.98 (s, 3H)., 7.17 (br s, 1H), 7.56−7.66 (m, 1H), 7.72 (t, J = 8.19 Hz, 1H), 7.85−7.93 (m, 2H), 13.36 (br s, 1H). HRMS: m/z (ES+) 343.0370 (MH^+) for $C_{14}H_9F_3N_2O_3S$.

6-(3-Bromophenyl)-4-(methylsulfinyl)-2-oxo-1,2-dihydropyridine-3-carbonitrile (37). ^{1}H NMR (300 MHz, DMSO-d_6) δ 2.80 (s, 3H), 7.15 (br s, 1H), 7.53−7.70 (m, 2H), 7.87 (d, J = 7.35 Hz, 1H), 8.00 (s, 1H), 13.18 (br s, 1H). HRMS: m/z (ES+) 336.9558 (MH^+) for $C_{13}H_9BrN_2O_2S$.

6-(3-Bromophenyl)-4-(methylsulfonyl)-2-oxo-1,2-dihydropyridine-3-carbonitrile (38). ^{1}H NMR (300 MHz, DMSO-d_6) δ 2.97 (s, 3H), 7.15 (br s, 1H), 7.53−7.70 (m, 2H), 7.87 (d, J = 7.35 Hz, 1H), 8.00 (s, 1H), 13.18 (br s, 1H). HRMS: m/z (ES+) 352.9517 (MH^+) for $C_{13}H_9BrN_2O_3S$.

6-(3-(Isopentyloxy)phenyl)-4-(methylsulfinyl)-2-oxo-1,2-dihydropyridine-3-carbonitrile (39). ^{1}H NMR (300 MHz, DMSO-d_6) δ 0.96 (d, J = 6.59 Hz, 6H), 1.65 (q, J = 6.78 Hz, 2H), 1.82 (td, J = 6.55, 13.28 Hz, 1H), 2.97 (s, 3H), 4.11 (t, J = 6.50 Hz, 2H), 7.17−7.25 (m, 2H), 7.40−7.60 (m, 3H), 12.78 (br, s, 1H). HRMS: m/z (ES+) 345.1284 (MH^+) for $C_{18}H_{20}N_2O_3S$.

6-(3-(3-Chlorobenzyloxy)phenyl)-4-(methylsulfonyl)-2-oxo-1,2-dihydropyridine-3-carbonitrile (40). ^{1}H NMR (300 MHz, DMSO-d_6) δ 3.49 (s, 3H), 5.24 (s, 2H), 7.27−7.35 (m, 2H), 7.39−7.58 (m, 6H), 7.62(br s, 1H), 12.78 (br, s, 1H). HRMS: m/z (ES+) 415.0321 (MH^+) for $C_{20}H_{15}ClN_2O_4S$.

6-(3-(4-Isopropylbenzyloxy)phenyl)-4-(methylsulfinyl)-2-oxo-1,2-dihydropyridine-3-carbonitrile (41). ^{1}H NMR (300 MHz, DMSO-d_6) δ 1.21 (d, J = 6.97 Hz, 6H), 2.82−2.93 (m, 1H), 2.97 (s, 3H), 5.17 (s, 2H), 7.06 (br s, 1H), 7.19−7.32 (m, 3H), 7.36−7.43 (m, 2H), 7.43−7.51 (m, 2H), 7.55 (s, 1H), 13.15 (br s, 1H). HRMS: m/z (ES+) 406.13511 (MH^+) for $C_{23}H_{22}N_2O_3S$.

6-(3-Bromophenyl)-4-(methylsulfonyl)pyridin-2(1*H*)-one (42). ^{1}H NMR (300 MHz, DMSO-d_6) δ 2.97 (s, 3H), 6.95 (s, 1H), 7.40−7.50 (m, 2H), 7.87 (d, J = 7.35 Hz, 1H), 8.02 (d, J = 7.35 Hz, 1H), 8.20 (s, 1H), 11.50 (br s, 1H). HRMS: m/z (ES+) 327.9565 (MH^+) for $C_{12}H_{10}BrNO_3S$.

4-(Methylsulfonyl)-2-oxo-1,5-dihydro-2*H*-chromeno[4,3-*b*]-pyridine-3-carbonitrile (43). ^{1}H NMR (300 MHz, DMSO d_6) δ 2.98 (s, 3H), 4.76 (br s, 2H), 6.97−7.09 (m, 1H), 7.20 (t, J = 7.63 Hz, 1H), 7.59−7.75 (m, 1H), 8.03 (t, J = 7.91 Hz, 1H), 12.72 (br s, 1H). HRMS: m/z (ES+) 303.0282 (MH^+) for $C_{14}H_{10}N_2O_4S$.

Determination of Mtb TMK IC_{50}. Mtb TMK activity was measured using a pyruvate kinase−lactate dehydrogenase (PK-LDH) coupled assay. A previously reported assay[15] was modified and adapted for the Mtb enzyme in 384-well format. All reactions were performed at 37 °C. Enzyme inhibition studies were done in a 75 μL reaction mixture containing 50 mM HEPES−NaOH (pH 7.5), 75 mM KCl, 2 mM DTT, 0.13 mM EDTA, 0.002% Brij, 0.5 mM phosphoenol pyruvate (PEP), 0.3 mM NADH, 10 U/mL PK-LDH, and 2 nM Mtb TMK. The reaction was started with the addition of $MgCl_2$ (to a final concentration of 5 mM) to the reaction mix. Change in absorbance at 340 nm (NADH consumption) was monitored for 120 min in a SpectraMax (Molecular Devices, Sunnyvale, CA) spectrophotometer.

The screening assay contained 1 μL of DMSO in the complete reaction wells (maximum signal), 20 mM EDTA in the blank reaction wells, and various concentrations of the test compound dissolved in DMSO in the test wells. The percentage inhibition values were calculated as the amount of enzyme activity inhibited in the test wells as compared to the complete reaction wells. EC_{50} values were calculated by plotting the calculated percentage inhibition values against the logarithm of inhibitor concentration. The data analysis was done using Excel-fit4 software (ID Business Solutions Ltd., U.K.) by nonlinear regression (curve fitting). The EC_{50} of the compound is calculated from the regression fit as the test compound concentration at which 50% inhibition of the enzyme activity is observed.

Determination of Whole Cell Activity against Mtb (Mtb MIC). All test compound stocks and dilutions were prepared in DMSO. Mtb MICs of test compounds were determined in 7H9 medium by the standard microdilution method[16] with some modifications. Briefly, 1 μL of serial 2-fold dilutions of test compound was dispensed in a 384-well microtiter plate (Corning 3702) at final concentrations ranging from 100 to 0.19 μM. An amount of 40 μL ((3−7) × 10^5 CFU/mL) of the bacterial culture was added to all the wells except the media control wells. Control wells included media and culture controls. The plates were packed in gas permeable polythene bags and incubated at 37 °C for 5 days. Following this incubation period, 8 μL of a freshly prepared 1:1 mixture of resazurin (0.02% in water) and 10% Tween 80 was added to all the wells. The plates were reincubated for an additional 24 h at 37 °C, and the color conversion of all wells was recorded. MIC is defined as the lowest drug concentration that prevented the color change from blue to pink. In order to determine the MICs, absorbance was monitored at 575 and 610 nm and their ratio calculated. By use of the ratio values, the media control and the no inhibitor/culture controls are assigned as equivalent to 100% and 0% inhibition, respectively. Within the concentrations screened with the test compounds, the least concentration that yielded 80% inhibition was considered as MIC.

Human Thymidylate Kinase (Hu TMK) Assay. Activity was assayed in the reverse direction by measuring the conversion of dTDP to dTMP with concomitant conversion of ADP to ATP. The production of ATP was coupled to *E. coli* D-ala-D-ala ligase A (DdlA), and the inorganic phosphate thus produced was measured using Malachite green reagent. The assay mixture consisted of 50 μM dTDP, 2 μM ADP and was initiated by addition of 50 nM Hu TMK, 500 nM *E. coli* DdlA in 50 mM HEPES−NaOH, pH 7.5, 25 mM KCl, 5 mM dithiothreitol, 10 mM $MgCl_2$, 0.01% Triton X-100, 10 mM D-alanine. The assay was performed in a final assay volume of 30 μL and incubated for 60 min at room temperature in 384-well clear microtiter plates (Matrix no. 4310). Malachite green reagent (45 μL) was added postincubation and absorbance was read at 650 nm.

Protein Nuclear Magnetic Resonance (NMR) Spectroscopy. The ^{15}N-labeled Mtb TMK samples were produced in *E. coli* using M9 minimal media supplemented with 5 g/L Celtone base powder (^{15}N, 98%; Cambridge Isotope Laboratories, Inc.). The protein was purified using immobilized metal affinity chromatography (NiNTA, QIAGEN) followed by size exclusion chromatography (SEC) using a Superdex75 column (GE Healthcare). The purified protein sequence comprises the native Mtb TMK sequence followed by three histidine residues. NMR spectra were recorded at 298 K on a Bruker Avance 600 MHz

DOI: 10.1021/jm5012947
J. Med. Chem. 2015, 58, 753−766

spectrometer running Topspin 1.3 equipped with a 5 mm TCI Cryoprobe with *Z*-axis gradients. The Mtb TMK samples for compound screening and subsequent compound titration comprised 0.1 mM ^{15}N-labeled protein in 500 μL of 50 mM Tris, pH 7.5, 50 mM NaCl, 1 mM TCEP, and 0.02% NaN_3. Compounds were screened in mixtures of 6 at a final concentration of 1.0 mM of each compound by diluting from 200 mM stock solutions in DMSO-d_6 into the sample. Binding was detected by ^{1}H−^{15}N 2D TROSY (transverse relaxation optimized spectroscopy)[17] spectra of the protein (F2xF1) 2048 × 50 complex pairs (in echo−antiecho mode), 12019 × 2000 Hz sweep width, 85.3 ms × 25.0 ms acquisition times. Mixtures were considered to contain a hit if peaks in the spectrum were shifted with respect to a reference spectrum by $^1/_2$ of the line width.

The binding component of a mixture was identified by recording a 200 ms mixing time $T_{1\rho}$ filtered 1D NMR spectrum[18] of the mixture (0.2 mM per compound) (1) without protein and (2) after addition of the protein (8 μM). Binding ligands are attenuated in spectrum 2 and revealed in the difference spectrum, (spectrum 2) − (spectrum 1). The active component was then identified by comparing the difference spectrum with reference spectra for each of the components.

Compound titrations were recorded from fresh compound stocks made up at 100 mM in DMSO-d_6, and spectra were recorded at typical ligand concentrations of 0.2, 0.6, 1.2, and 2.0 mM. The affinity of the compounds was determined via simultaneous nonlinear fitting of chemical shift perturbations, typically for at least three residues, versus compound concentration using the law of mass action.

Protein Expression and Purification. Two variants of Mtb TMK were used for crystallization. These were untagged, full length Mtb TMK and a truncated variant referred to as C2 which lacks the four C-terminal residues.

Proteins were expressed in *E. coli* BL21* grown in LB media in the presence of ampicillin (100 μg/mL). Cells were initially grown at 37 °C until OD_{600} = 0.6 was reached, at which point cells were cooled to 25 °C, induced with IPTG, and growth allowed to continue for 20 h before harvesting by centrifugation. Cells were resuspended in lysis buffer (50 mM Tris-HCl, pH 7.5, 150 mM NaCl, 0.1 mM EDTA, 0.25 mg/mL lysozyme) supplemented with EDTA free Complete protease inhibitors (Roche). Cells were lysed using a cell disruptor (Constant Systems Basic Z). The lysate was centrifuged at 35 000 rpm (100 000*g*) for 60 min using a Beckman ultracentrifuge. The cleared supernatant was loaded onto 40 mL of Blue Sepharose resin which had been equilibrated with lysis buffer. The resin was then washed with 3 × 40 mL buffer A (150 mM NaCl, 50 mM Tris-HCl, pH 7.5, 0.1 mM EDTA). TMK was eluted using a gradient of increasing NaCl up to 500 mM. The peak from the Blue Sepharose column containing TMK was further purified by size exclusion chromatography on a Superdex 26/60 (GE Healthcare) equilibrated with 50 mM Na HEPES, pH 7.5, 150 mM NaCl, 10% glycerol, 0.1 mM EDTA, 1 mM DTT. Fractions corresponding to the peak containing TMK were pooled and concentrated to 20−40 mg/mL.

Protein Crystallization, X-ray Diffraction Data Collection, Structure Solution, Model Building, and Refinement. Protein/inhibitor complexes were prepared by adding 100 mM compound stock solution in 100% DMSO to protein to a final concentration of 1 mM compound. The resulting complexes were crystallized using the hanging drop method by mixing 2 μL of well solution with 2 μL of protein/inhibitor complex solution. Detailed protein crystallization conditions are provided in Supporting Information S7, Table S7-1. X-ray diffraction data were collected from cryocooled crystals at the ESRF or in-house as detailed in Supporting Information S7, Table S7-2. Data were integrated, scaled, merged, and reduced using programs from the CCP4 suite.[19] Structures were solved by molecular replacement using AmoRe[18] with PDB 1G3U as the search model. Structures were refined using iterative cycles of manual model building in Coot[20] interspersed with reciprocal space refinement in Refmac.[21] Detwinning was applied where necessary. Statistics of the data collection, refinement, and final model quality are provided in Supporting Information S7, Table S7-2.

■ ASSOCIATED CONTENT

Ⓢ Supporting Information

Druggability assessment, molecular docking, predicted pK_a, comparison of kinases, inhibitory activity, protein expression and purification, and protein crystallographic data. This material is available free of charge via the Internet at http://pubs.acs.org.

Accession Codes

Atomic coordinates and structure factors for Mtb TMK in complex with compounds **8**, **23**, **28**, **33**, and **36** have been deposited in the Protein Data Bank (PDB accession codes 4unn, 4unr, 4unp, 4uns and 4unq, respectively).

■ AUTHOR INFORMATION

Corresponding Authors

*M.P.: e-mail, manapanda@gmail.com; phone, +91-9663384657.

*J.R.: e-mail, Jon.Read@astrazeneca.com; phone, +44 (0)1625 510661.

Present Address

⊥J.A.T.: Northern Institute for Cancer Research, Paul O'Gorman Building, Medical School, Newcastle University, Framlington Place, Newcastle upon Tyne, NE2 4HH, UK.

Notes

The authors declare no competing financial interest.

■ ACKNOWLEDGMENTS

The authors acknowledge the contributions from scientists involved in construct design and protein expression and purification. The authors thank Tanjore S. Balganesh, Bala Subramanian, and Kaveri Das for their constant support and encouragement.

■ ABBREVIATIONS USED

TB, tuberculosis; Mtb, *Mycobacterium tuberculosis*; TMK, thymidylate kinase; TMP, thymidine monophosphate; NiNTA, nickel nitriloacetic acid; SAR, structure−activity relationship; NMR, nuclear magnetic resonance; HTS, high-throughput screening; SAR, structure−activity relationship; FBLG, fragment based lead generation; LE, ligand efficiency; LLE, lipophilic ligand efficiency; FRIT, fragment hit; rt, room temperature; NHAC, number of heavy (non-hydrogen) atom counts; TROSY, transverse relaxation optimized spectroscopy; MIC, minimum inhibitory concentration

■ REFERENCES

(1) (a) Zumla, A.; Nahid, P.; Cole, S. T. Advances in the development of new tuberculosis drugs and treatment regimens. *Nat. Rev. Drug Discovery* **2013**, *12*, 388−404. (b) LeChartier, B.; Rybniker, J.; Zumla, A.; Cole, S. T. Tuberculosis drug discovery in post genomic era. *EMBO Mol. Med.* **2014**, *6*, 158−168. (c) Barry, C. E. Lessons from seven decades of antitubercular drug discovery. *Curr. Top. Med. Chem.* **2011**, *11*, 1216−1225.

(2) (a) Sassetti, C. M.; Boyd, D. H.; Rubin, E. J. Genes required for mycobacterial growth defined by high density mutagenesis. *Mol. Microbiol.* **2003**, *48*, 77−84. (b) Sassetti, C. M.; Rubin, E. J. Genetic requirements for mycobacterial survival during infection. *Proc. Natl. Acad. Sci. U.S.A.* **2003**, *100*, 12989−12994.

(3) (a) Xiong, X.; Xu, Z.; Yang, Z.; Liu, Y.; Wang, D.; Dong, M.; Parker, E. J.; Zhu, W. Key targets and relevant inhibitors for the drug discovery of tuberculosis. *Curr. Drug Targets* **2013**, *14*, 676−699. (b) Ballel, L.; Field, R. A.; Duncan, K.; Young, R. J. New small-molecule synthetic antimycobacterials. *Antimicrob. Agents Chemother.*

DOI: 10.1021/jm5012947
J. Med. Chem. 2015, 58, 753−766

2005, *49*, 2153−2163. (c) Janin, Y. L. Antituberculosis drugs: ten years of research. *Bioorg. Med. Chem.* **2007**, *15*, 2479−2513.
(4) Van Calenbergh, S.; Pochet, S.; Munier-Lehmann, H. Drug design and identification of potent leads against *Mycobacterium tuberculosis* thymidine monophosphate kinase. *Curr. Top. Med. Chem.* **2012**, *12*, 694−705.
(5) (a) Li de la Sierra, I.; Munier-Lehmann, H.; Gilles, A. M.; Barzu, O.; Delarue, M. X-ray structure of TMP kinase from Mycobacterium tuberculosis complexed with TMP at 1.95 Å resolution. *J. Mol. Biol.* **2001**, *311*, 87−100. (b) Fioravanti, E.; Adam, V.; Munier-Lehmann, H.; Bourgeois, D. The crystal structure of *Mycobacterium tuberculosis* thymidylate kinase in complex with 3′-azidodeoxythymidine monophosphate suggests a mechanism for competitive inhibition. *Biochemistry* **2005**, *44*, 130−137. (c) Fioravanti, E.; Haouz, A.; Ursby, T.; Munier-Lehmann, H.; Delarue, M.; Bourgeois, D. *Mycobacterium tuberculosis* thymidylate kinase: structural studies of intermediates along the reaction pathway. *J. Mol. Biol.* **2003**, *327*, 1077−1092.
(6) (a) Keating, T. A.; Newman, J. V.; Olivier, N. B.; Otterson, L. G.; Andrews, B.; Boriack-Sjodin, P. A.; Breen, J. N.; Doig, P.; Dumas, J.; Gangl, E.; Green, O. M.; Guler, S. Y.; Hentemann, M. F.; Joseph-McCarthy, D.; Kawatkar, S.; Kutschke, A.; Loch, J. T.; McKenzie, A. R.; Pradeepan, S.; Prasad, S.; Martinez-Botella, G. In vivo validation of thymidylate kinase (TMK) with a rationally designed, selective antibacterial compound. *ACS Chem. Biol.* **2012**, *7*, 1866−1872. (b) Martinez-Botella, G.; Breen, J. N.; Duffy, J. E. S.; Dumas, J.; Geng, B.; Gowers, I. K.; Green, O. M.; Guler, S.; Hentemann, M. F.; Hernandez-Juan, F. A.; Joseph-McCarthy, D.; Kawatkar, S.; Larsen, N. A.; Lazari, O.; Loch, J.; Macritchie, J. A.; McKenzie, A. R.; Newman, J. V.; Olivier, N. B.; Otterson, L. G.; Owens, A. P.; Read, J.; Sheppard, D. W.; Keating, T. A. Discovery of selective and potent inhibitors of Gram-positive bacterial thymidylate kinase (TMK). *J. Med. Chem.* **2012**, *55*, 10010−10021.
(7) Choi, J. Y.; Plummer, M. S.; Starr, J.; Desbonnet, C. R.; Soutter, H.; Chang, J.; Miller, J. R.; Dillman, K.; Miller, A. A.; Roush, W. R. Structure guided development of novel thymidine mimetics targeting *Pseudomonas aeruginosa* thymidylate kinase: from hit to lead generation. *J. Med. Chem.* **2012**, *55*, 852−870.
(8) Cui, H.; Carrero-Lerida, J.; Silva, A. P. G.; Whittingham, J. L.; Brannigan, J. A.; Ruiz-Perez, L. M.; Read, K. D.; Wilson, K. S.; Gonzalez-Pacanowska, D.; Gilbert, I. H. Synthesis and evaluation of α-thymidine analogs as novel antimalarials. *J. Med. Chem.* **2012**, *55*, 10948−10957.
(9) (a) Toti, K. S.; Verbeke, F.; Risseeuw, M. D. P.; Frecer, V.; Munier-Lehmann, H.; Van Calenbergh, S. Synthesis and evaluation of 5′-modified thymidines and 5-hydroxymethyl-2′-deoxyuridines as *Mycobacterium tuberculosis* thymidylate kinase inhibitors. *Bioorg. Med. Chem.* **2013**, *21*, 257−268. (b) Vanheusden, V.; Munier-Lehmann, H.; Froeyen, M.; Dugué, L.; Heyerick, A.; De Keukeleire, D.; Pochet, S.; Busson, R.; Herdewijn, P.; Van Calenbergh, S. 3′-C-branched-chain-substituted nucleosides and nucleotides as potent inhibitors of *Mycobacterium tuberculosis* thymidine monophosphate kinase. *J. Med. Chem.* **2003**, *46*, 3811−3821.
(10) (a) Gasse, C.; Douguet, D.; Huteau, V.; Marchal, G.; Munier-Lehmann, H.; Pochet, S. Substituted benzyl-pyrimidines targeting thymidine monophosphate kinase of *Mycobacterium tuberculosis*: synthesis and in vitro anti-mycobacterial activity. *Bioorg. Med. Chem.* **2008**, *16*, 6075−6085. (b) Familiar, O.; Munier-Lehmann, H.; Ainsa, J. A.; Camarasa, M.-J.; Perez-Perez, M.-J. Design, synthesis and inhibitory activity against *Mycobacterium tuberculosis* thymidine monophosphate kinase of acyclic nucleoside analogs with a distal imidazoquinolinone. *Eur. J. Med. Chem.* **2010**, *45*, 5910−5918.
(11) (a) Halgreen, T. J. Identifying and characterizing binding sites and assessing druggability. *J. Chem. Inf. Model.* **2009**, *49*, 377−389. (b) *SiteMap*, version 2.6; Schrödinger, LLC: New York, NY, 2012.
(12) ligand efficiency (LE) = $(-RT \ln K_i)$/(no. of heavy atom counts) = −0.592[ln(IC_{50} in molar)/(no. of heavy atom counts)]. Lipophilic ligand efficiency (LLE) = pIC_{50} − calculated log *D*.
(13) Hopkins, A. L.; Keseru, G. M.; Lesson, P. D.; Rees, D. C.; Reynolds, C. H. The role of ligand efficiency matrices in drug discovery. *Nat. Rev. Drug Discovery* **2014**, *13*, 105−121.
(14) (a) Singh, B.; Lesher, G. Y. A facile and novel synthesis of 1,6-naphthyridin-2-(1*H*)-ones. *J. Heterocycl. Chem.* **1990**, *27*, 2085−2091. (b) Cook, B. N.; Eldrup, A. B.; Mugge, I. A.; Soleymanzadeh, F.; Sun, S.; Zhang, Y. Preparation of substituted [1,6]naphthyridine derivatives as urotensin II receptor antagonists. PCT Int. Appl. WO 2008144268 A1, 2008 (Boehringer Ingelheim, Germany). (c) Ratcliffe, A. H.; Pearce, R. J.; Gibson, K. H.; Wood, R.; Masek, B. B. Naphthyridine derivatives as angiotensin II inhibitors. Eur. Pat. Appl. EP0516392 A2, 1992.
(15) Blondin, C.; Serina, L.; Wiesmuller, L.; Gilles, A. M.; Barzu, O. Improved spectrophotometric assay of nucleoside monophosphate kinase activity using the pyruvate kinase/lactate dehydrogenase coupling system. *Anal. Biochem.* **1994**, *220*, 219−221.
(16) Franzblau, S. G.; Witzig, R. S.; McLaughlin, J. C.; Torres, P.; Madico, G.; Hernandez, A.; Degnan, M. T.; Cook, M. B.; Quenzer, V. K.; Ferguson, R. M.; Gilman, R. H. Rapid, low-technology MIC determination with clinical *Mycobacterium tuberculosis* isolates by using the microplate Alamar Blue assay. *J. Clin. Microbiol.* **1998**, *36*, 362−366.
(17) Pervushin, K. V.; Wider, G.; Wuthrich, K. Single transition-to-single transition polarization transfer (ST2-PT) in [^{15}N,^{1}H]-TROSY. *J. Biomol. NMR* **1998**, *12*, 345−348.
(18) Hajduk, P. J.; Edward, T.; Olejniczak, E. T.; Fesik, S. W. One-dimensional relaxation- and diffusion-edited NMR methods for screening compounds that bind to macromolecules. *J. Am. Chem. Soc.* **1997**, *119*, 12257−12261.
(19) The CCP4 suite: programs for protein crystallography. *Acta Crystallogr., Sect. D* **1994**, *50*, 760−763.
(20) Emsley, P.; Cowtan, K. Coot: model-building tools for molecular graphics. *Acta Crystallogr., Sect. D* **2004**, *60*, 2126−2132.
(21) Refmac version 5.1.17: Murshudov, G. N.; Vagin, A. A.; Dodson, E. J. Refinement of macromolecular structures by the maximum-likelihood method. *Acta Crystallogr., Sect. D* **1997**, *53*, 240−255.

DOI: 10.1021/jm5012947
J. Med. Chem. 2015, 58, 753−766